New sorption compressor designs for the METIS cooler in the E-ELT

Master Thesis Applied Physics

by T. Mulder

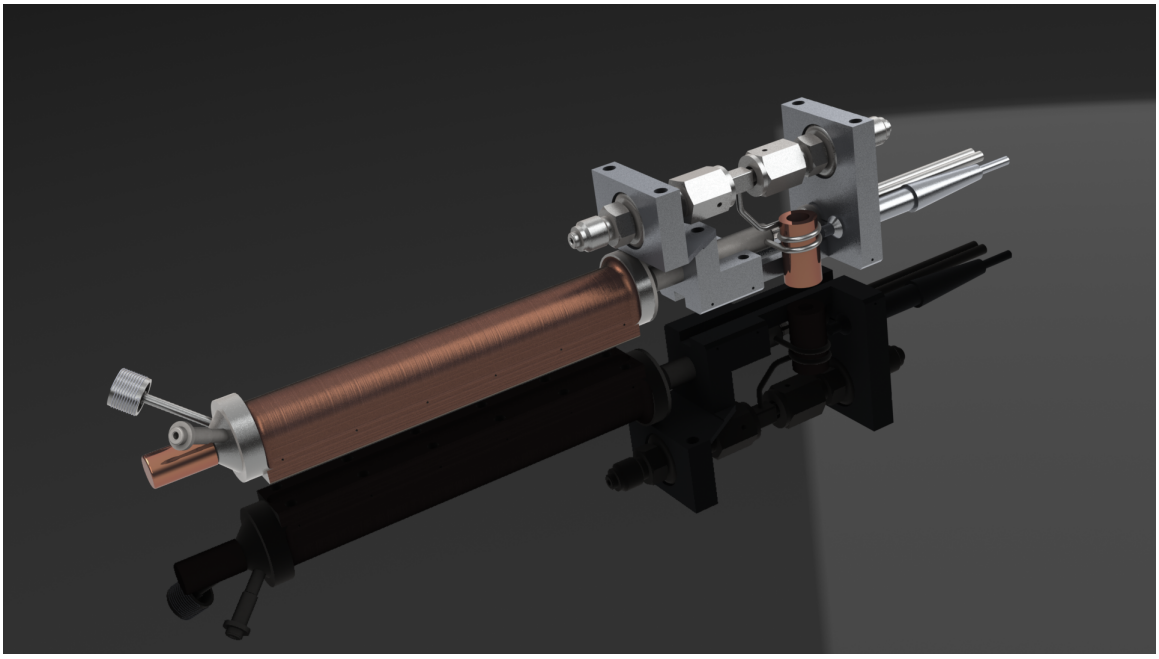

Energy, Materials and Systems group
University of Twente
Enschede, The Netherlands

March 10, 2014

Committee:
Prof dr. ir. H.J.M. ter Brake
Assoc. prof. dr. C. Sun
Dr. ir. S. Vanapalli
MSc. Y. Wu

UNIVERSITY OF TWENTE.

EMSE

Abstract

Sorption-based cooling provides vibration free and electro-magnetic interference free cooling that fits the needs of space applications and ultra sensitive sensors. In sorption compressors for space applications efficiency is of most importance, therefore Gas-Gap Heat Switches (GGHS) are used to limit the energy loss during operation. For the METIS instrument in the European Extremely Large Telescope, a ground based application, efficiency is of lower concern. For this reason new sorption compressor designs are made for the cooling system of this instrument. In these new designs the primary change is the replacement of the GGHS by a layer of insulation. To evaluate the performance of the new compressor design a dynamic thermal model is developed. This model simulates the behavior of a sorption compressor cell and provides values for the cycle time, required input power and the amount of mass it can deliver. The results of the model are validated by experiments. The new compressor cell design is optimized for the compressor system in the METIS cooler by using the model. The optimized compressor system includes 70 new compressor cells with a total required input power of 1093 W. This is an 31% increase in input power compared a compressor system that uses compressor cells with the old design that include gas-gap heat switches. However, the new design will increase the manufacturability and lower the production costs of the sorption compressor cells.

Contents

1 Introduction

Cooling of space-applications and ultra-sensitive sensors is a delicate matter. Conventional cooling systems often use compressors that cause vibrations and electro magnetic interference (EMI), reducing the performance of the cold instruments. These compressors contain moving parts which have the disadvantage to wear over time and thus limit the lifetime of the cooler. A few types of vibration free cooling systems exist today. One of these systems uses sorption-based Joule-Thomson cooling [1]. Although this cooling technique is vibration and EMI free, it lacks in efficiency compared to Stirling or pulse-tube cooling.

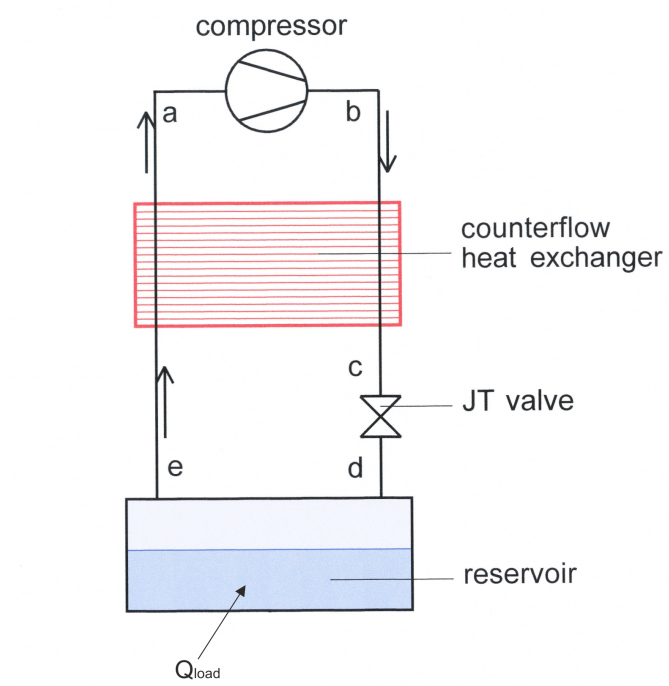

Figure 1.1: A schematic overview of a closed cycle JT cooler [2]

1.1 Joule-Thomson Refrigeration

Sorption coolers combine sorption compressors with a Joule-Thomson (JT) cold stage. The steady flow of a working gas and counterflow heat exchangers are used in the JT cold stage to achieve cooling [2]. JT coolers can be used in small and large scale cooling systems and are often used in the liquefaction of gases. A schematic overview of a typical closed cycle JT cooler is presented in Figure 1.1. The compressor in a sorption cooler will consists out of a system containing multiple sorption compressor cells. Other components in a typical JT cooler include of a counterflow heat exchanger, a JT-valve and a reservoir.

The principle behind JT cooling is the isenthalpic expansion of a pressurized gas in the JT-valve. This expansion often corresponds with a change in temperature of the working gas [3]. Below the inversion temperature of the gas, corresponding to the high pressure before the JT-valve (state c in Figure 1.1), the gas cools on expansion to a lower temperature. In some cases, the gas on expansion results into a co-existence region of the substance forming partly liquid. This liquid can exchange heat from the surroundings to form gas. This is the gross refrigeration capacity of the cooler.
The sorption compressor system in the cooler will provide the required pressure difference that drives the steady flow of the gas in the cooler. A more detailed explanation on how a sorption compressor cell works is given in section 1.3.

In the counterflow heat exchanger heat is exchanged between the cold low pressure gas and the warm high pressure gas. Counterflow heat exchangers usually consist of two tubes with a thermal connection between them. The cold gas in one tube will pre-cool the warm high pressure gas in the other tube. The high pressure gas will exit the counterflow heat exchanger at a lower temperature. Isenthalpic expansion of this pre-cooled gas in the JT-valve will result in lower temperatures that can be reached.

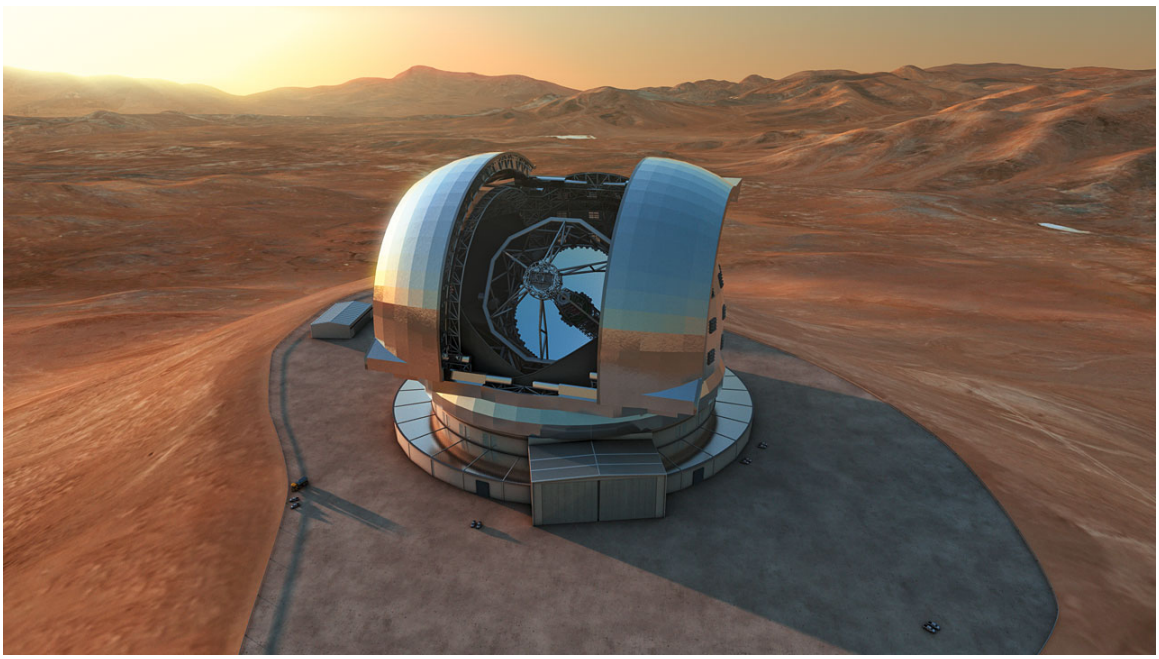

Figure 1.2: An artist's impression of the E-ELT [6]

1.2 European Extremely Large Telescope

Sorption cooling is already used in space applications, *i.e.* the Planck mission [4] and the proposed Darwin mission [5], but sorption cooling also becomes more and more popular for ground-based applications. One of the ground-based applications for which a sorption cooler is being developed is the European Extremely Large Telescope (E-ELT).

The E-ELT is a project of the European Southern Observatory (ESO). When finished, this telescope will be the largest optical telescope in the world with a main mirror diameter of 39 meters. The telescope is planned to be operational in the early 2020s. An artist's impression of the E-ELT on its building site at Cerro Armazones, Chile is presented in Figure 1.2. The telescope houses eight instruments and two post-focal modules. These instruments will perform extensive studies on topics including exoplanets, the formation of primordial objects in space, black holes, dark matter and dark energy [6–11].

One of the instruments in the E-ELT is called *METIS*, which stands for "Mid-infrared ELT Imager and Spectrograph". This instrument detects mid-IR electromagnetic radiation of 3 to 14 μm to, among others, determine physical and chemical properties of exoplanets [11]. METIS itself contains multiple instruments that detect and image the LM- and N-band. These instruments operate at four different temperature levels [12], provided in table 1.1, and require a very low level of vibrations. Because of the vibration requirement of these instruments, the choice was made to develop a sorption cooling system, that can cool the instruments to their corresponding temperature levels.

METIS Instrument	*Maximum required temperature (K)*
Radiation shield	85
Fore Optics	85
Cold Calibration Unit	85
Wave Front Sensor	85
LM-Imager	85
LM-Spectrometer	85
LM-Band Detectors	40
N-Band Imager	25
N-Band Detector	8

Table 1.1: Maximum required temperatures for the components in the METIS instrument [12]

The development of the sorption cooler for the METIS instrument is performed by the University of Twente in collaboration with Dutch Space. The University of Twente has more than 10 years experience developing sorption coolers for different types of applications. For this particular application a three stage sorption cooler is being designed. The instruments with maximum temperature requirements higher than 40 K are cooled directly by liquid nitrogen, the other levels are cooled by the three cold stages of the sorption cooler. A schematic overview of the design of the METIS sorption cooler chain is presented in Figure 1.3. The first stage of the cooler is the neon stage, with a cold-end that reaches 40 K. This stage cools the LM-band detector and also pre-cools the second stage of the cooler. The second stage is a hydrogen stage with two JT restrictions to reach 25 K and 15 K. The 25 K bath will be used to cool the N-band imager. Both the 25 K and the 15 K bath are used to pre-cool the third stage of the cooler. The hydrogen compressor system uses a two-stage configuration to build up the required pressure ratio. The last stage is a helium stage that will reach 8 K to cool the N-band detector. The sorption compressors in cooler also require cooling. This is establishes with a thermal link between the compressors and the bath of liquid nitrogen. Why sorption compressors need to be cooled is explained in the next section.

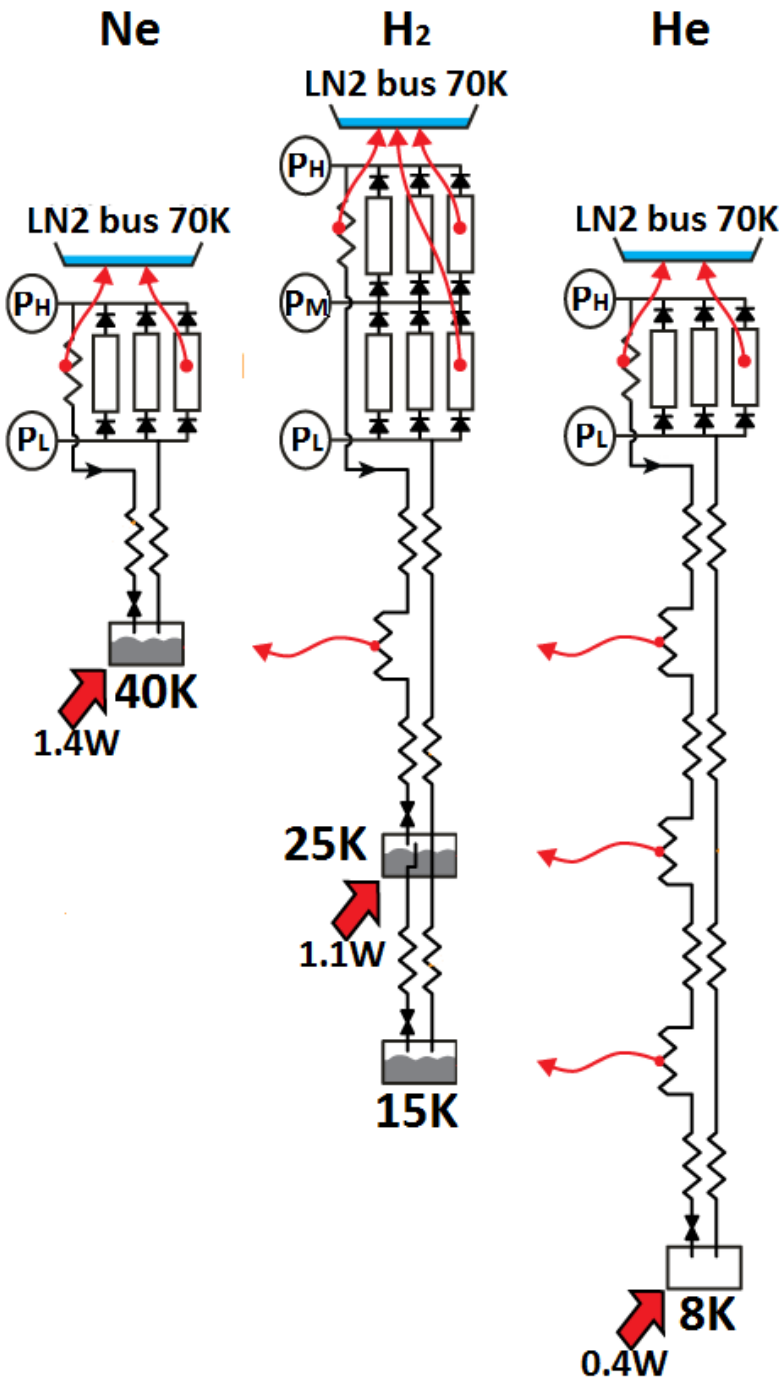

Figure 1.3: Schematic overview of the METIS cooler chain [12]

1.3 Sorption Compressors

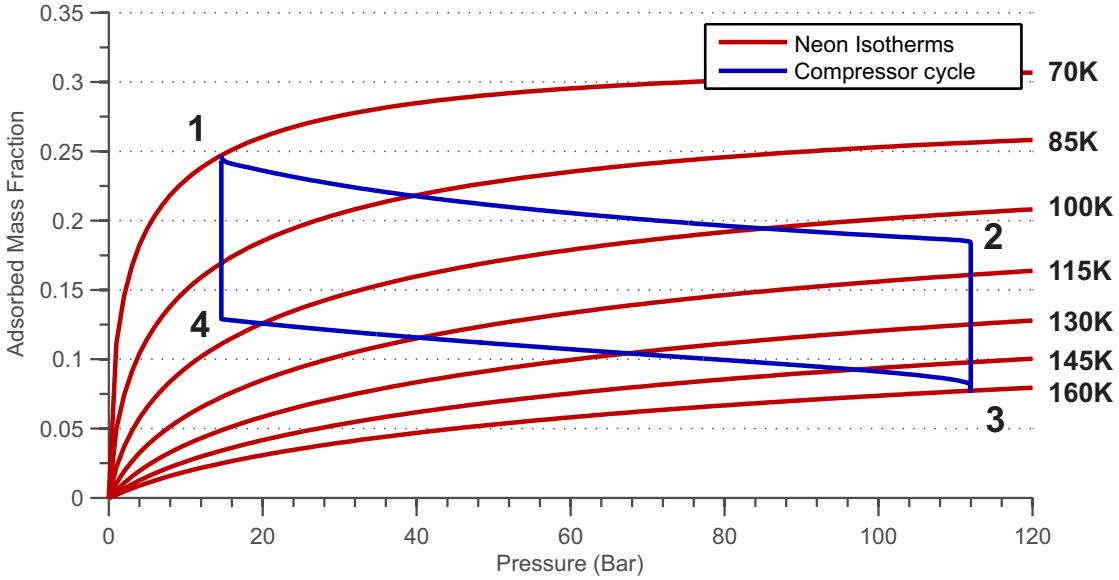

Figure 1.4: Typical adsorption isotherms of neon on saran carbon (red), including an example of a sorption cycle of a neon compressor cell (blue).

The sorption compressors that are used in this project contain activated-carbon that allows the physical adsorption of gas [13]. These compressors operate on the basis of a thermal cycle, an example of a typical cycle of a compressor using neon gas is presented in Figure 1.4. In this figure the amount of adsorbed neon onto the carbon is plotted as a function of the pressure for different isothermal lines. An increase in pressure or a decrease in temperature allows more gas to be adsorbed onto to carbon.

The compression cycle starts at a low temperature and at a low pressure (point 1 in Figure 1.4). Pressure is build up in the compressor at constant volume by heating the carbon and causing the desorption of gas (1->2). Check valves open at a threshold pressure and allow the desorbed gas to flow out of the compressor and into the high pressure buffer at a constant pressure (2->3). In this phase the temperature will still increase. After most gas is desorbed from the carbon, the heater is turned off and the compressor will start to cool down again. At this point all check valve are closed. Cooling down will cause the gas in the compressor to be adsorbed onto the carbon and the pressure will drop (3->4). When the pressure has reached its initial value, the check valve to the low-pressure buffer will open. Gas from this buffer will flow into the compressor and is adsorbed by the carbon while it cools down at constant pressure (4->1). When the compressor is back at its starting temperature, a new cycle can be initiated. Since mass-flow out of the compressor is only established for a limited time (point 2 to point 3 in this cycle), usually multiple compressor cells are connected in parallel and operated out of phase to establish continuous mass-flow. A typical cycle time of a sorption compressor is in the order of minutes.

A schematic overview of a standard sorption compressor design is presented in Figure 1.5. In the center of the compressor there is an internal heater, which is used to heat the carbon. The heater

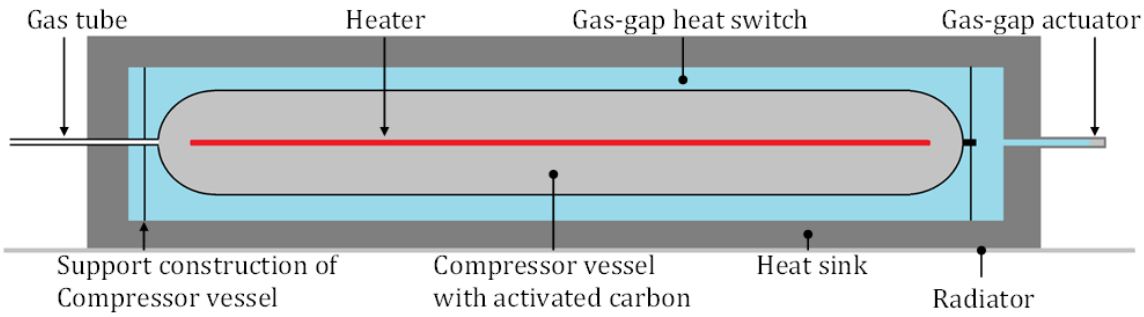

Figure 1.5: A schematic overview of a standard sorption compressor with a gas-gap heat switch.

itself is surrounded by cylindrical carbon pills. The carbon pills are firmly packed inside a container to prevent the gas from entering the gas-gap. The container is surrounded by a Gas-Gap Heat Switch (GGHS) to minimize heat losses during heating. During heating the GGHS will be pumped to vacuum, limiting the conductive heat-flow from the carbon to the heat sink. During the cool down phase, the GGHS will be filled with gas to increase the thermal conduction and thus increase the heat-flow to the heat sink. Vacuuming and filling the GGHS is accomplished by a small piece of adsorbent called a *gas-gap actuator* that adsorbs and desorbs the working gas of the GGHS.
In the cooling system for METIS, the compressors are 50 cm long and cooled by liquid nitrogen. To increase the performance of the compressor cells, the liquid nitrogen is pumped down to 70K, increasing the amount of gas a compressor cell is able to adsorb.

For space applications the efficiency is an important aspect of a compressor, because the size of the radiator scales with the inefficiency. For ground-based compressors, like the sorption compressors that are developed for the METIS cooler, efficiency is of lower concern. This opens an opportunity to make a new sorption compressor design that is easier to manufacture and has a lower production cost compared to the current designs.

1.4 Scope of this Thesis

In this thesis new design concepts will be explored in the development of the sorption compressor systems for the METIS cooler. This primarily includes replacing the gas-gap heat switch by a layer of insulation. Although a GGHS increases the efficiency of a compressor, it is not a mandatory part. The efficiency of the compressor will decrease by replacing the GGHS by a layer of insulation. However, this replacement will have a positive effect on the manufacturability and it lowers the production costs of a compressor cell. Another topic of exploration is the position of the heater. In the original design the position of the heater is in the center of the carbon, but other positions are possible and will be evaluated. A compressor system that uses a new design still has to meet the requirements set for this cooling system. These requirements are based on a statical analysis of the METIS cooler performed by Y. Wu [14]. This analysis not only provides pressure and mass-flow requirements for the compressor system, but also derived an input power for the compressor system if gas-gap heat switches are used. This total input power, including a 10% margin, is determined to be 832 W. A more detailed overview of the system requirements is provided in table 1.2.

The final goal of this thesis is to design a compressor system for the METIS cooler chain that is easy to manufacture and relatively cheap to build without increasing the input power too much compared to the original compressor system design using gas-gap heat switches.

Stage	*Helium*	*Neon*	*Hydrogen*
Working Fluid	He-4	Ne	H2
Carbon	Saran	Saran	Saran
Heat Sink Temperature (K)	70	70	70
Low Pressure (Bar)	7.50	13.6	0.122
Intermediate Pressure (Bar)	-	-	2.00
High Pressure (Bar)	14.3	112	23.8
Mass-flow (mg/s)	101.4	148.5	8.343
Input Power (W)	524	175	133

Table 1.2: Requirements for, and properties of the compressor systems in the METIS cooler [14]. The input power presented in this table is for a compressor system that uses sorption compressors with a gas-gap heat switch.

2 New Concepts

Initially the sorption compressors designs for the METIS cooler chain included gas-gap heat switches (GGHS). The GGHSs increase the efficiency of the compressors, but for the ground-based compressors in the METIS cooler chain these heat switches are not mandatory. Since a GGHS is quite difficult to manufacture and is an expensive part of the compressor cell, the choice is made to explore other options.

The primary subject of exploration is the replacement of the GGHS by a layer of insulation. This new option has a lower production cost and is easier to manufacture, but will create a continuous heat-flow to the heat sink during the heating process, reducing the efficiency of the compressor. The material of this insulation layer should have a low thermal conductivity in range of the operating temperatures of the compressors and, also important, it should not be porous. If the insulation material is a porous material, it cannot contain the gas within the carbon, which increases the void volume inside the compressor. This means a container must be placed between the carbon and the insulation layer to contain the gas inside the carbon. Adding a container will increase the heat capacity of the warm part of the compressor, causing the compressor to have a slight decrease in efficiency. A literary study reveals the most suitable materials for the layer of insulation are Kapton and Teflon [15, 18]. Both are non-porous, easily available and not expensive. Of the two materials, Kapton has the lowest thermal conductivity and is expected to achieve the best results.

Another geometry related option is looking at other locations for the heater. Originally the heater is placed in the center of the cylindrical carbon pills, but there are several other positions where the heater might have better heating capabilities. For example, placing the heater on the outside of the carbon gives the heater a larger contact area to the carbon, but also a larger contact area to the insulation, creating a large heat leak to the heat sink.

To evaluate these options, the compressor is divided into four key sections:

1. Heater
2. Activated carbon
3. Insulation / GGHS
4. Heat sink

With these sections four different configurations are designed, these configurations are presented in Figure 2.1. The first three configurations are new concepts, the last configuration is the original compressor design that uses a GGHS and will be used as reference in the evaluation of the new designs.

1 - Heater in the center
The first configuration is most similar to the original design, only the gas-gap and container are replaced by a layer of non-porous insulation. Since all heat will flow through the carbon, this is expected to be the most efficient configuration of the three new configurations.

2 - Heater on the outside
In this configuration the heater is located on the outside of the carbon, this means a larger contact area between the carbon and the heater, but also a larger heat leak to the heat sink. Since not all heat will flow through the carbon, significant losses are expected.

3 - Heater in the center and on the outside
This configuration is a combination of the first two configurations that hopefully has the efficiency of the first design and the heating capabilities of the second design. By controlling the ratio of heating power between the inner and outer heater, a uniform temperature distribution is expected.

4 - Original design
This is the original design of the sorption compressor with a gas-gap heat switch and will be used as reference for the other three designs.

Other configurations, such as a spiraling heater through the carbon will not be explored. Configurations like those are difficult to manufacture and that is something that needs to be avoided.

To evaluate the different concepts, a dynamic thermal model is developed, that is capable of simulating among others the heat-flow, pressure build-up and mass-flow of a sorption compressor. In the next chapter this model will be explained in detail.

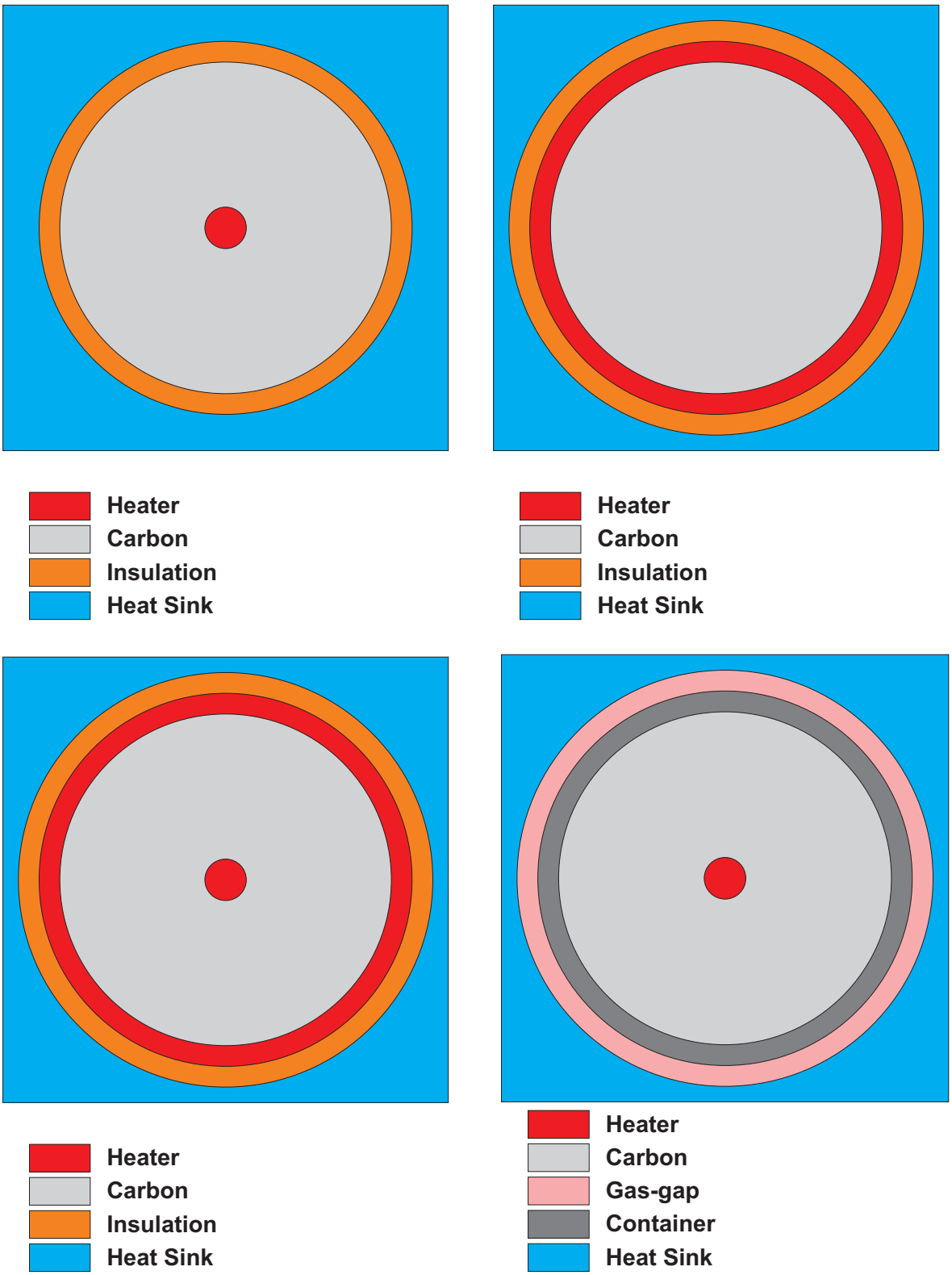

Figure 2.1: The four different configurations that will be evaluated with the thermal model.

3 Thermal Model

A 1-dimensional dynamic thermal model is developed in Matlab to predict the performance of a compressor cell according to the configurations described in Chapter 2. This model will also be used in the design of the new compressor systems for the METIS cooler. The model runs on a modified version of a delayed differential equation solver called *dde15s* [16]. This solver uses the Matlab ordinary differential equation solver *ode15s*, but adds the possibility to access solutions as a function of previous times. *ode15s* is a stiff differential equation solver, this means it is able to solve equations that give unstable results using standard numerical solving methods. Heat transfer equations are considered to be stiff [17] and so need to be solved by this type of solver.
The dynamic thermal model can be split into two sub-models. The first sub-model is a *closed* model, which means that the gas cannot leave the compressor. The second sub-model is an *open* model, which allows the gas to flow in and out of the compressor when threshold pressures are reached. The results have to be validated in order to use the dynamic thermal model in the design of the compressor systems for the METIS cooler. For large parts both models run on the same scripts, for this reason the validation of one model also validates the other model to a large extend. The validation is achieved by two types of experiments, these experiments are explained in Chapter 4. Only the second model is used in the evaluation of the different configurations and the design of the compressor systems for the METIS cooler. The first model is merely used because the validation experiment is easy to set up.

3.1 Physical aspects of the simulation

In the models the sorption compressors are thermically driven, that means a change in temperature drives the adsorption and desorption of gas. The primary heat source is the heater. Additional heat is generated by the change in the amount of adsorbed mass and the change in pressure. The heat will transfer only via conduction from the warm compressor cell to the cold heat sink. The convective and radiative terms in these models are neglected.
To simulate the thermal flow in the compressor, the different sections are split into ring-shaped elements. Sections with a low thermal conductivity, like the carbon and the insulation, are split into multiple elements. For sections with a high thermal conductivity one ring-shaped element is sufficient. For each element, the model keeps track of the temperature. For each carbon element the model also keeps track of the amount of adsorbed gas in that particular ring. The material properties of the different sections are received from Ekin [18], NIST [19] and measurements performed at the University of Twente.

In the following subsections the physics in the different sections of the simulated compressor are described.

3.1.1 Heater

A schematic overview of the inner heater, as found in configuration 1, 3 and 4, is presented in Figure 3.1. The heater is the part of the compressor that achieves the highest temperature and is also the part with the highest thermal conductivity. The heat coming into the heater consists of the generated ohmic heat, expressed by Equation 3.1, and, in case the heater is not in the middle of the compressor, the heat conducted into the heater during the cool down phase. Since the thermal conductivity of the heater is three orders of magnitude larger than the thermal conductivity of the carbon and the layer of insulation, the heat conduction out of the heater can be reduced to only the conduction from the edge of the heater to the middle of the first carbon ring, expressed by Equation 3.2.

$$\dot{q}_{generated} = G\pi r_1^2 L \tag{3.1}$$

$$\dot{q}_{conduction} = 2\pi L k_c \frac{T_1 - T_h}{ln(r_{12}/r_1)} \tag{3.2}$$

Here G is the heat generated per volume, L is the length of the compressor and k_c is the thermal conductivity of the carbon. Combining both the ohmic heat and the heat conducted out of the heater, an expression for the temperature is derived:

$$dT = \frac{\dot{q}_{generated} + \dot{q}_{conduction}}{\rho\pi r_1^2 Lc} dt \tag{3.3}$$

Here ρ and c are the density and the heat capacity of the heater. This equation can be rewritten as:

$$dT = \frac{\dot{q}_{generated} + \dot{q}_{conduction}}{Mc} dt \tag{3.4}$$

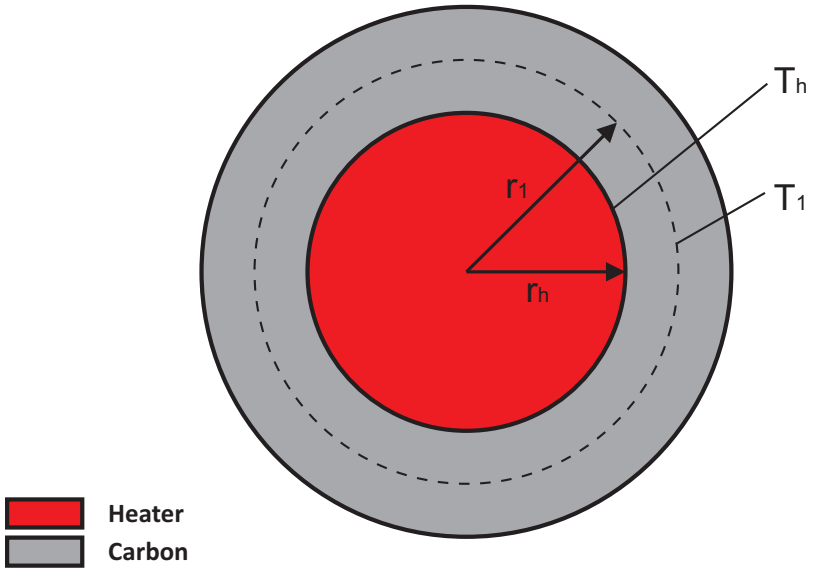

Figure 3.1: Schematic overview of the heater and first ring of the carbon

3.1.2 Carbon

The simulated carbon section of the compressor consists out of multiple rings and for each ring the model keeps track of the temperature and the amount of adsorbed gas.

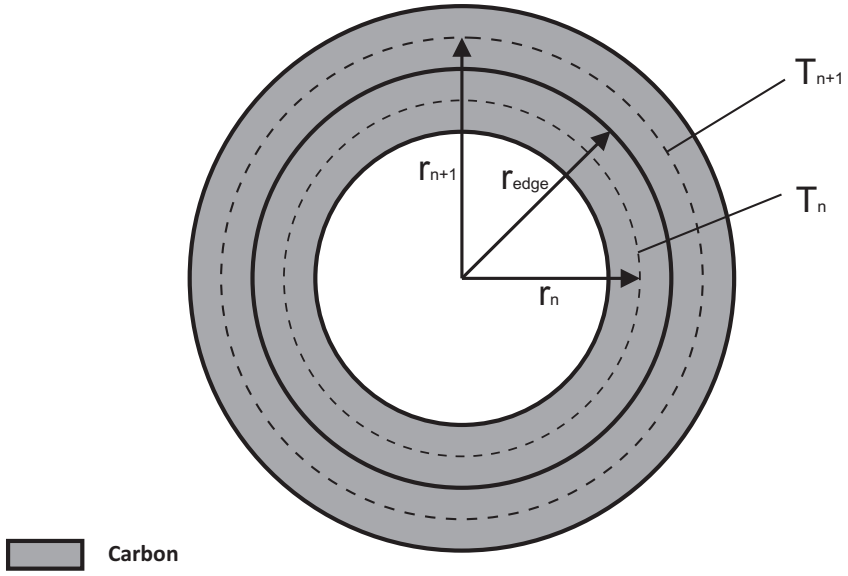

Figure 3.2: Schematic overview of two carbon rings

In Figure 3.2 a schematic overview of two carbon rings that are connected to each-other is presented. The thermal resistance between the two rings is given by the temperature dependent thermal resistance from the middle of the inner ring to the edge of the middle ring, plus the thermal resistance from this edge to the middle of the outer ring:

$$R_{total} = R_n + R_{n+1} = \frac{ln(r_{edge}/r_n)}{2\pi L k_n} + \frac{ln(r_{n+1}/r_{edge})}{2\pi L k_{n+1}} \tag{3.5}$$

Here k_n is the effective thermal conductivity of the porous carbon and L is the length of the compressor cell.

The method to calculate the effective thermal conductivity is based on a model for thermal conduction in a porous media described by D.A. Nield [20]. In this method the adsorbed gas is seen as a fluid that lays on the surface of the activated carbon. The effective thermal conductivity is a weighted geometric mean between thermal conductivity of the solid carbon and the thermal conductivity of the fluid:

$$k_{eff} = k_f^{\phi} k_s^{1-\phi} \tag{3.6}$$

Here ϕ is the porosity of the activated carbon, k_s is the thermal conductivity of the solid carbon and k_f is the thermal conductivity of the fluidic part. The thermal conductivity of the free gas is included in the thermal conductivity of the fluidic part of the medium. As an overview, the thermal conductivity of the carbon with different adsorbed gases as a function of the temperature is presented in Figure 3.3.

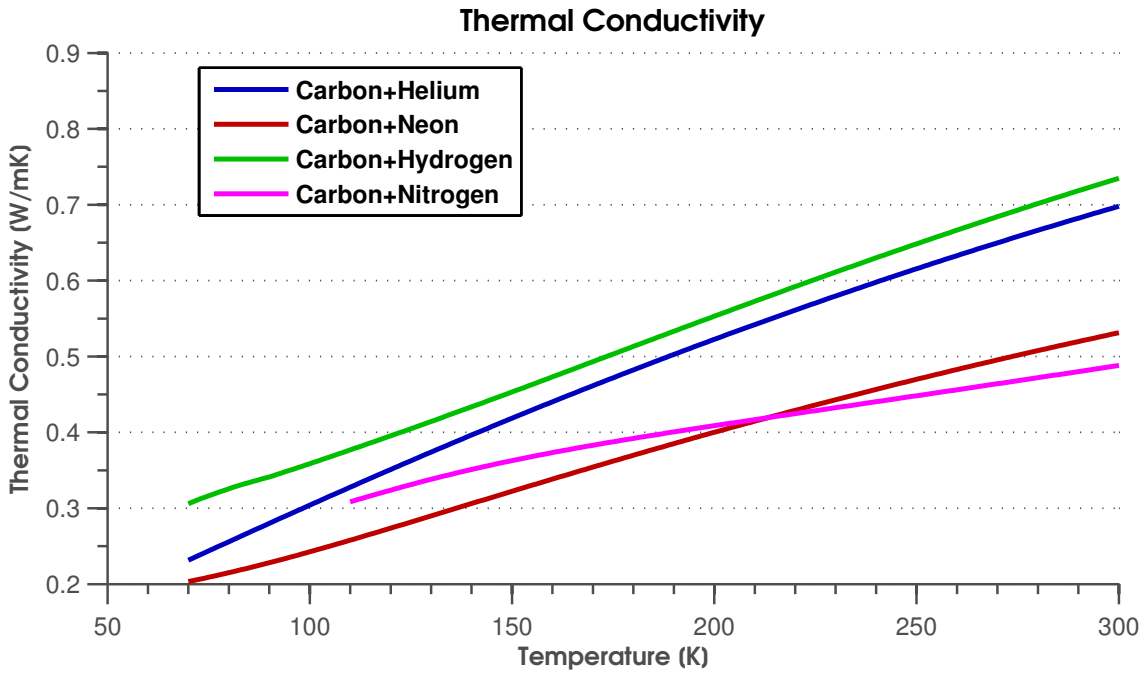

Figure 3.3: Thermal conductivity of the carbon with several adsorbed gases at 10 Bar. With this pressure nitrogen becomes liquid just below 110K, for this reason the temperature range of thermal conductivity of the carbon with nitrogen gas start at 110K.

Using the total thermal resistance from Equation 3.5, the heat-flow from one ring to the next ring is calculated as followed:

$$\dot{q}_{conduction} = \frac{1}{R_{tot}}(T_{n+1} - T_n) \tag{3.7}$$

The heat generated by the heater is the largest contribution to the change in temperature of the carbon in the compressor. However, there are two other terms that are included in the simulation. The first one is the heat of adsorption, given by Equation 3.8 [21, 22] and is directly derived from the adsorption isotherms. A Matlab script, provided by Y. Wu, calculating the heat of adsorption is integrated in the model.

$$\dot{q}_{ads} = M(\frac{-R}{M_{gas}}\frac{\partial ln(p/p_0)}{\partial(1/T)}|_{x_s})\frac{\partial x_s}{\partial t} = Mc_{x_s}\frac{\partial x_s}{\partial t} \tag{3.8}$$

Here R is the gas constant, M_{gas} is the molar mass of the working gas, p_0 is the standard pressure, M is the mass of the carbon element, x_s is the ratio of amount of adsorbed gas to the mass of the carbon and c_{x_s} is a coefficient linking the change in adsorption to the change in energy with the dimension J/kg.

The second contribution is the change in pressure that provides a small change in energy:

$$\dot{q}_P = Mc_P\frac{\partial P}{\partial t} \tag{3.9}$$

Here c_P is a coefficient linking the change in pressure to the change in energy with the dimension Jms^2kg^{-2}.

The total change in energy of one carbon ring is given by the following equation:

$$\dot{q}_{tot} = \dot{q}_{conduction} + \dot{q}_{ads} + \dot{q}_P \tag{3.10}$$

Using this change in energy the change in temperature is calculated by the following equation:

$$dT = \frac{\dot{q}_{tot}}{Mc} dt \tag{3.11}$$

Where c is the total heat capacity of the carbon, fluid and gas:

$$c = c_{carbon} + c_{fluid} + c_{gas} \tag{3.12}$$

In the dynamic thermal model the convection of the gas is not taken into account; this includes the warm gas warming cold parts of the carbon during the heating phase and the cold gas cooling the carbon during filling. Since at both moments convection speeds up the current process, slightly better results are expected if convection is included. Still, the amount of heat convection could transfer is small compared to all other energy terms and for that reason the convective terms are neglected without reducing the integrity of the model.

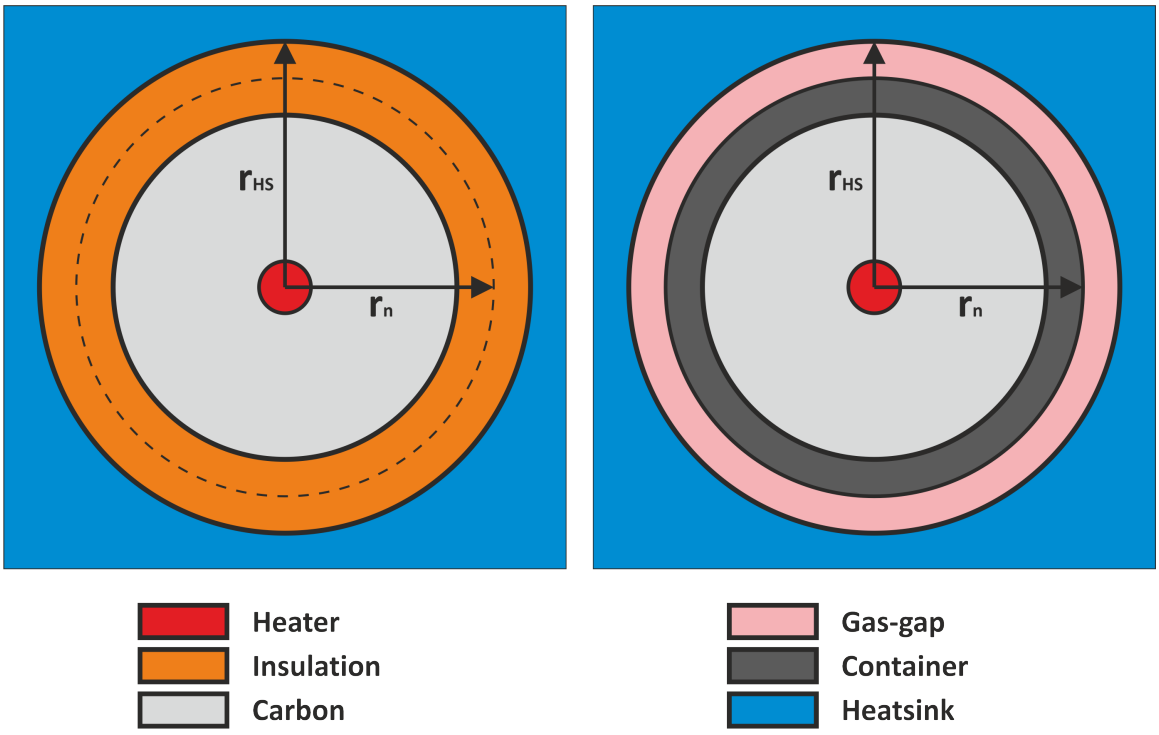

Figure 3.4: Schematic overview of the insulation and the heat sink

3.1.3 Insulation and the Gas-Gap Heat Switch

The insulation and the gas-gap heat switch are the last parts between the compressor and the heat sink. A schematic overview of the insulation and gas-gap is presented in Figure 3.4. There is no heat production in both parts, so the only heat coming in and going out is through conduction. The layer of insulation is divided into multiple rings. The temperature and the conduction of heat for each ring is calculated using the same method as described in subsection 3.1.2.
For simplicity, the gas-gap only has a value for its thermal conductivity and the heat is instantly transported to the other side of the gap. In both cases the thermal resistance of the last ring to the heat sink is calculated using the following equation:

$$R_{out} = \frac{ln(r_{HS}/r_n)}{2\pi L k_n} \tag{3.13}$$

With this thermal resistance the heat-flow to the heat sink is calculated using Equation 3.7. In all cases the temperature of the heat sink is considered constant.

3.1.4 Pressure, Mass and Adsorption Ratio

At the start of the simulation, the total amount of gas that is in the compressor is calculated using the adsorption isotherms. The mass of the gas in the compressor can be seen as a function of the temperature, pressure and the mass of the carbon. The total mass of the gas includes the mass of the adsorbed gas and the mass of the free gas. The mass of the adsorbed gas, M_{ads}, is given by the following equations:

$$M_{ads} = V_{carbon}\rho_{carbon}(1-\phi)X_{ads}(T,P) \tag{3.14}$$

$$M_{ads} = M_{carbon}X_{ads}(T,P) \tag{3.15}$$

Where X_{ads} is the ratio between the amount of adsorbed gas and the mass of the carbon, V is the total volume of the carbon, ρ is the density and ϕ is the porosity of the carbon. The value for X_{ads} is derived from measured adsorption isotherms and material properties. Matlab scripts calculating these ratio's from the isotherms are provided by Y. Wu and integrated into the model.

The same method is used to calculated the mass of the free gas in the compressor cell:

$$M_{gas} = M_{carbon}(\frac{\rho_{gas}\phi}{\rho_{carbon}(1-\phi)} - \frac{\rho_{gas}X_{ads}(T,P)}{\rho_{ads}}) \tag{3.16}$$

$$M_{gas} = M_{carbon}X_{gas}(T,P) \tag{3.17}$$

Here the mass of the free gas is derived from the volume ratio between the free gas and the carbon minus the volume fraction of the adsorbed gas. The total mass of the gas is the sum of M_{ads} and M_{gas}.

$$M_{tot} = M_{carbon}X_{tot}(T,P) = M_{ads} + M_{gas} \tag{3.18}$$

In the simulation of a closed system the total mass of the gas is conserved. That means the sum of the mass of the gas in all carbon rings must always be equal to the total mass of the gas that was present at the start of the simulation.

$$M_{tot} = \sum_{n=1}^{N} M_{carbon} X_{tot,n}(T_n, P) \tag{3.19}$$

In the model it is assumed that the pressure in all sections of the compressor has the same value. Since the total mass of the gas in the compressor and the temperature of each carbon ring is known, Equation 3.19 can be solved to find the pressure in the compressor.

In simulations of an open compressor the total mass of the gas in the compressor cell changes over time. A check-valve opens at a given high-pressure allowing the gas to flow out of the compressor and another check-valve opens at a low-pressure letting cold gas flow into the compressor. In this case the Matlab-solver keeps track of the total mass in the system. Using the same method as described above, the pressure in the compressor is calculated.

3.1.5 Check-valves and Buffers

In the compressor simulation the check-valves behave as ideal check-valves, that means there is no cracking pressure, hysteresis and pressure drop over the valves. Also the model used ideal buffer, they have an infinite volume, so the pressure in the buffer is stable at the specified pressure.
As mentioned before, the simulation is thermically driven, that means the pressure is calculated using the temperature profile. When the calculated pressure is higher than the pressure in the high-pressure-buffer, the pressure in the compressor will be set to the buffer pressure. Using Equation 3.19, the new total mass of the gas in the compressor is calculated. The same method is used when the pressure drops below the pressure of the low-pressure-buffer. The flowchart in Figure 3.5 illustrates this method.

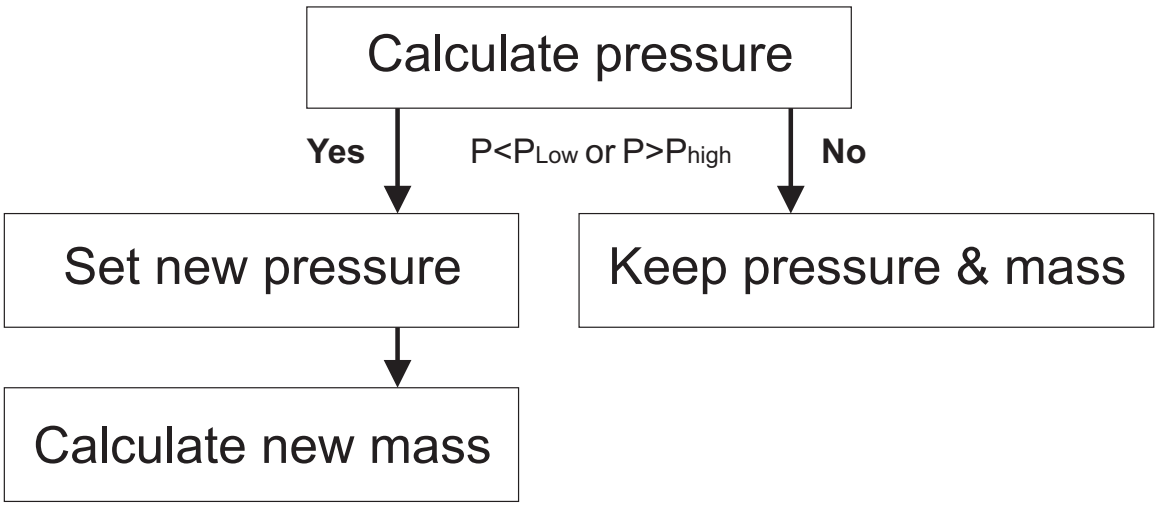

Figure 3.5: A flowchart describing the method that is used to evaluate if mass-flow is established and to calculate the new gas mass in the compressor cell.

3.2 Simulation Results

The four different compressor cell configurations are simulated using similar geometric and operating settings as the helium stage in the METIS cooler and the results are discussed in this section. The thermal model is also used to design the compressor systems for the three stages of the METIS cooler, this will be discussed in Chapter 5. Here, the main points of interests are the average mass-flow, the cycle time and the input power. These are discussed below.

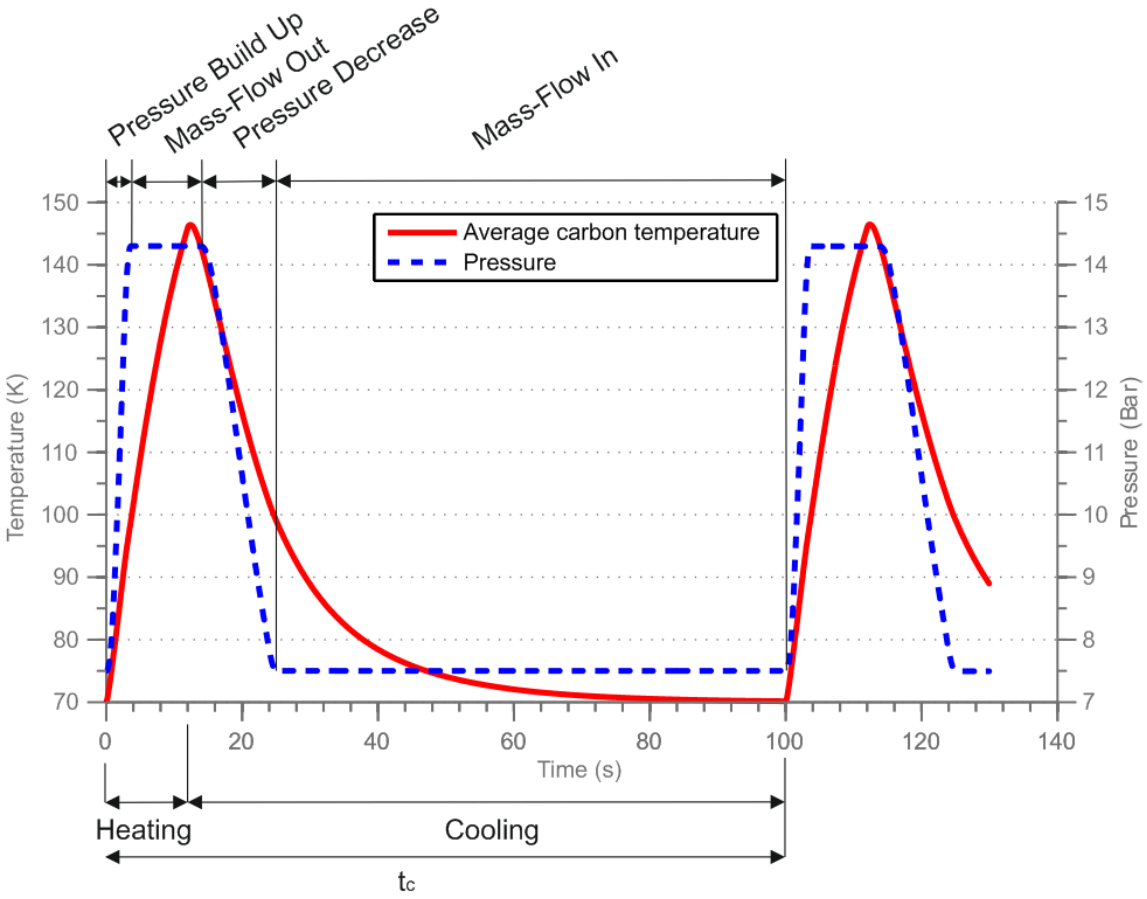

Figure 3.6: The simulated average temperature of the carbon and the pressure inside a sorption compressor cell as a function of time. Heating is applied for 12 seconds. The different phases of the compression cycle are labeled. The average temperature of the carbon still increases after the heater has stopped, this is caused by the redistribution of heat in combination with temperature dependent heat capacity of the carbon.

3.2.1 Mass-flow

In order for the compressor to start a new cycle, the carbon has to resorb the amount of gas it delivered to the high-pressure buffer. The time it takes for the compressor to deliver and to resorb this amount of gas is called the cycle time. In Figure 3.6, the different phases of a sorption cycle are illustrated by using the average temperature of the carbon and the pressure inside the compressor as an example.

As can be seen in the figure, a sorption compressor does not provide continuous mass-flow to the buffer. Mass-flow out of the compressor is only established in a small time-frame at a high flow. The average mass-flow of a compressor cell is given by:

$$\dot{m}_{avg} = \frac{\triangle m}{t_c} \tag{3.20}$$

Here $\triangle m$ is the total mass delivered by a compressor cell during one cycle and t_c is the cycle time. With the average mass-flow per compressor cell and the mass-flow requirement of the compressor system the total amount of compressor cells in the system can be calculated:

$$N = \frac{\dot{m}_{tot}}{\dot{m}_{avg}} = \frac{\dot{m}_{tot} t_c}{\triangle m} \tag{3.21}$$

The number of compressor cells in the system is a function $\triangle m$ and t_c. The total mass delivered per cycle, $\triangle m$, is also a function of t_c. Figure 3.7 illustrates the relation between the total mass delivered and the cycle time. The choice of the cycle time will lead to a certain number of compressor cells.

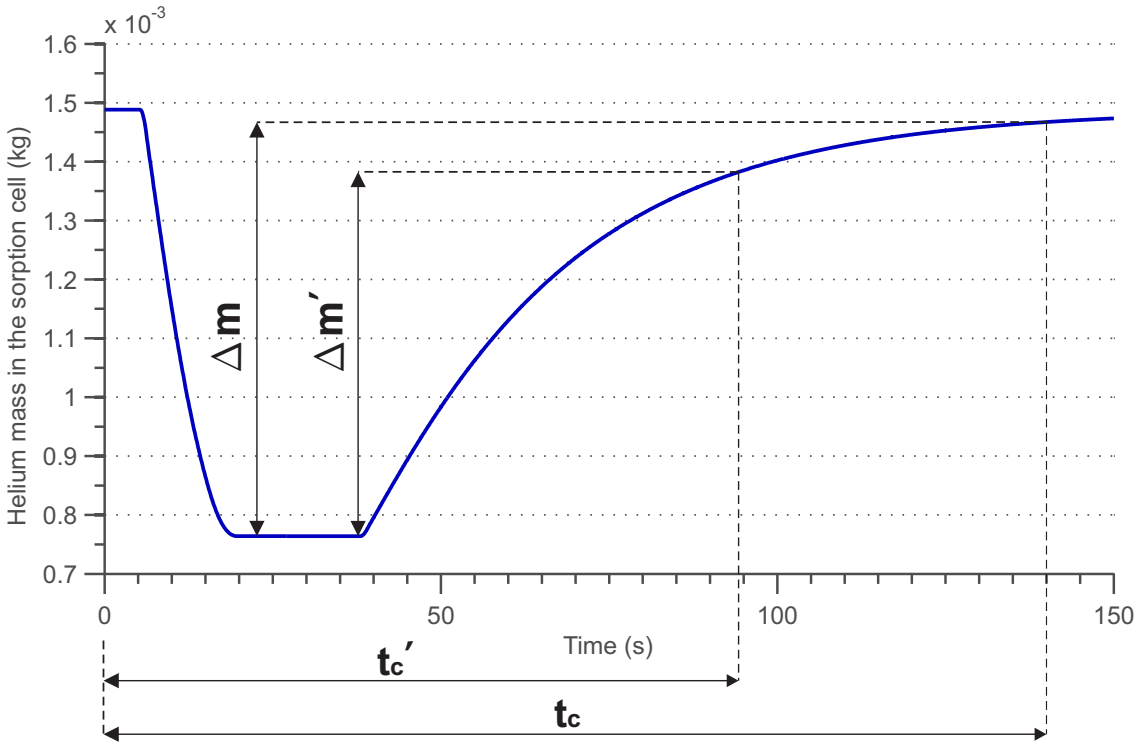

Figure 3.7: Helium mass in a simulated 1 meter long compressor cell as a function of time. At the start of the cycle, the carbon is at 70K. In the figure two different cycle times are chosen, both correspond to a certain mass the compressor can deliver per cycle.

3.2.2 Input Power

The average input power of a compressor cell is given by:

$$P_{avg} = \frac{P_h t_h}{t_c} \tag{3.22}$$

Here P_h is the heating power and t_h is the heating time. The total input power for a compressor system can be expressed by the number of compressor cells in that system multiplied with the average input power per cell:

$$P_{tot} = \frac{N P_h t_h}{t_c} = \frac{\dot{m}_{tot} P_h t_h}{\triangle m} \tag{3.23}$$

In each cycle in the simulation, the heating power and heating time are fixed, for that reason the total input power will only be a function of the total mass delivered per cycle, $\triangle m$, and thus the input power will be a function of the cycle time, see Figure 3.7. From Equation 3.23 can be inferred that an increase in $\triangle m$ per cycle will directly result in a decrease in input power.

To characterize the performance of a single compressor cell, one can best look at the amount of mass that can be delivered per Joule of input energy:

$$FOM = \frac{\triangle m}{P_h t_h} \tag{3.24}$$

This figure of merit gives a good measure of the efficiency of the compressor cell.

As an example, two different cycle times are chosen in Figure 3.7, t_c and t_c'. These cycle times correspond to the total mass delivered per cycle $\triangle m$ and $\triangle m'$. Of the two cycle times, t_c is the longest and corresponds to the largest delivered mass per cycle. For that reason the input power of the compressor system using t_c as cycle time will be lower than the input power of the compressor system using t_c'.
In this example, the average mass-flow per cell is larger if the cycle time t_c' is chosen:

$$\frac{\triangle m'}{t_c'} > \frac{\triangle m}{t_c} \tag{3.25}$$

$$\dot{m}_{avg}' > \dot{m}_{avg} \tag{3.26}$$

This means less compressor cells are needed by selecting t_c' as cycle time. However, the mass delivered per cycle $\triangle m'$ is lower than $\triangle m$, which results into a larger input power for the compressor system using t_c'. If the selected cycle time becomes too low, almost no mass can be delivered per cycle. This causes an increase in the number of compressor cells. For this reason a minimum in the number of compressor cells of a compressor system can be found by selected the correct cycle time.

3.2.3 Cycle Time Selection

Choosing a cycle time will influence both the number of compressor cells and the total input power of the compressor system. Figure 3.7 clearly shows that choosing a longer cycle time will increase $\triangle m$ until the point where no extra mass is adsorbed. At this point, the carbon in the compressor has

reached the heat sink temperature and the end of its cycle. These long cycle times are needed if low input powers are required. However, for the total number of compressor cells it is better to choose a cycle time that does not allow the carbon to reach the heat sink temperature.

In the evaluation of the simulated compressor cells, the choice of the cycle time will be based on the simulated average temperature of the carbon. This means, that when the average temperature of the carbon drops below a certain temperature during the cool-down phase, a new cycle will be initiated. Simulations with very different average mass-flows and cycle times can be compared with each other by using this method. Preliminary simulations are analyzed in order to select this *critical* value for average temperature of the carbon.

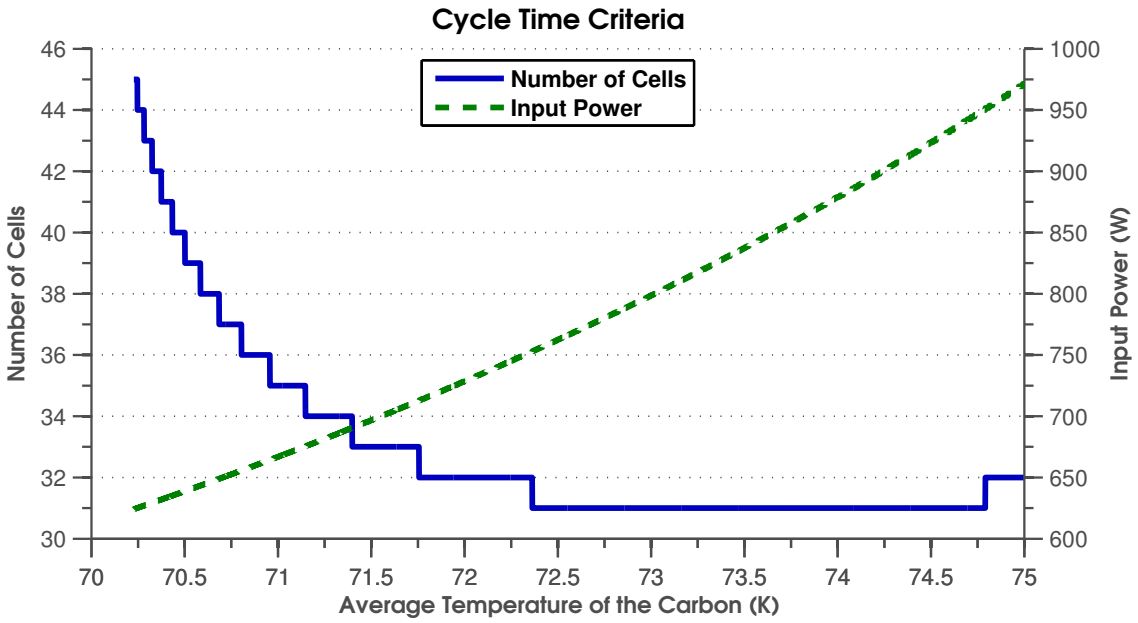

Figure 3.8: Number of compressor cells and total power of the helium stage as a function of the chosen critical average carbon temperature. The heat sink temperature is fixed at 70 K.

An example of one of the analyzed simulations is presented in Figure 3.8. In this figure the total number of compressor cells and total input power of a helium stage compressor system are presented as a function of the selected average carbon temperature. The heat sink temperature of this simulated compressor system is stable at 70 K. This figure illustrates that choosing a relatively high average carbon temperature (*i.e.* 73 K) on which a new cycle initiates will results in a low number of compressor cells needed, but requires a high input power. On the other hand, choosing a low average carbon temperature (*i.e.* 70.5 K) results in a low input power, but requires more compressor cells in the compressor system.
An average carbon temperature of 71 K is selected to be the cycle time criteria for the compressor systems in the METIS cooler. Using this value, a good balance between the number of compressor cells and total input power is found.

Since the compressor in the simulation is at 70 K at the start of the first cycle and the following cycles start at 71 K, slightly less heating is required in these next cycles. For that reason a correction will be

made in the found cycle time and in the applied heating time:

$$t_{h,corrected} = t_h - t_{71} \tag{3.27}$$

$$t_{c,corrected} = t_c - t_{71} \tag{3.28}$$

Here t_{71} is the time that is required to heat the carbon in the compressor from the heat sink temperature of 70 K to an average temperature of 71 K.

3.2.4 Evaluation of the New Configurations

The different configurations described in chapter 2 are simulated and their results are analyzed. The main points of interest in these analyses are the average mass-flow and the average input power per compressor cell. The operating parameters are fixed in all simulations, the geometry specific parameters can differ slightly between configurations. Table 3.1 provides an overview of these parameters. The total input energy per cycle is fixed at 3600 J. In all four configurations this is achieved by heating with 300 W for 12 seconds. 300 W/m is the largest power density the heater can provide and from preliminary simulations the best results are expected using this power density.

Parameters	*Value*
Heating time (s)	12
Heating power (W/m)	300
Heat sink Temperature (K)	70
Filling Pressure (Bar)	7.5
Low-Pressure buffer (Bar)	7.5
High-Pressure buffer (Bar)	14.3
Inner heater diameter (mm)	1
Carbon pill diameter (mm)	5
Insulation layer thickness (mm)	1
Compressor length (m)	1
Carbon	Saran
Working gas	Helium
Insulation	Kapton

Table 3.1: Parameters settings that are used in the simulations to compare the different configurations.

As a reminder, a schematic overview of the four different configurations is presented in Figure 3.10. Representative results for thes configurations during one compression cycle are presented in Figures 3.11 to 3.14 and a overview of the performance of the simulated compressors is provided in Table 3.2. All setups reach 14.3 Bar and are able to deliver mass-flow. A detailed analysis of the configurations is described below.

Configuration 1: Heater in the center

From the three new proposed configurations, this configuration can deliver the largest amount of mass per joule of input power. This efficient performance of the compressor cell is mainly because it can keep most of the heat inside the compressor during the heating phase (81.9%). This also allows high average temperatures of the carbon to be reached, see Figure 3.12. These high average temperatures are not found in configuration 2 and 3. What this configuration gains in the mass deliver per

Configuration	*1*	*2*	*3*	*4*
Average mass-flow (mg/s)	5.43	5.31	4.65	4.34
Average input power (W)	49.8	72.1	56.8	36.5
Total mass delivered (mg)	383	265	291	419
Cycle time (s)	70.5	49.9	62.6	96.3
Figure of merit (mg/J)	0.11	0.07	0.08	0.12
Heat lost during heating (%)	18.1	54.8	41.4	0.28

Table 3.2: Overview of the performance of the four different configurations.

Joule of energy and average mass-flow during a cycle, it loses in cycle time.
The temperature profiles over the compressors at the end of the heating phase are presented in Figure 3.15. Of the three new configurations, this configuration has the largest thermal gradient over the carbon. A thermal gradient allows the gas that is desorbed in the warm part of the carbon, to be adsorbed in the cold part, illustrated by Figure 3.9. This effect slows down the pressure build up in the compressor and causes a slight decrease in cell efficiency.

Configuration 2: Heater on the outside
To keep the heat capacity of the outer heater similar to the inner heater in the other configurations, the thickness of the outer heater is reduced to 25 micron.
Having the heater on the outside of the carbon means a larger contact area with the carbon, but also a larger contact area with the layer of insulation. This directly results in a larger heat leak to the heat sink and thus more heat losses during heating (54.8%) and a shorter cycle time, see Figure 3.13. Heating from the outside allows better heat distribution over the carbon, resulting in a lower temperature gradient over the carbon compared to the other configurations. Although this configuration has a low total mass delivered per cycle, the short cycle time allows a good average mass-flow to be reached. The total energy input per cycle is fixed and the cycle time of this configuration is very short, this results into a large average input power per compressor cell.

Configuration 3: Heater in the center and on the outside
Configuration 3 is a mix between the first two configurations. It can achieve a high total mass delivered by heating mostly with the inner heater or a short cycle time by heating mostly with the outer heater. Unfortunately it cannot achieve both at the same time. In this simulation 25% of the heat is generated in the inner heater and 75% of the heat in generated in the outer heater. By controlling the ratio of heating power between the inner and outer heater, one can control and thus reduce the temperature gradient over carbon, which results in a faster pressure build-up in the compressor, see Figure 3.11, and a higher mass to be delivered per cycle compared to configuration 2. For this reason, configuration 3 is preferred over configuration 2.

Configuration 4: Original compressor with a gas-gap heat switch
This configuration contains a container between the carbon and the gas-gap. Since the container has a large thermal conductivity and a large heat capacity, its presence has negative effect on the efficiency of the compressor. Despite of the container, this setup is able to deliver the largest amount

of mass per cycle and has the highest efficiency. To make a good comparison between this configuration and the three new configurations, the heating time is also set to 12 seconds. However, in the standard operation of sorption compressors with a gas-gas heat switch, usually longer heating with lower power is applied. This is required for the most efficient use of a compressor with a gas-gap. The extra mass that could be delivered by heating longer at a lower power is only a few percent higher than delivered mass in this simulation. This would increase the efficiency of the compressor cell, but decrease the average mass-flow.
At the start of the simulation the gas-gap is filled with 2 Pascal of hydrogen gas, after 16.5 seconds the gas gap pressure is increased to 400 Pascal. The values of the chosen pressures are consistent with the pressures used in actual sorption compressors with a gas-gap. During heating, most of the heat stays in the compressor, for this reason this configuration reaches the highest average carbon temperature of all configurations. The hydrogen gas in the gas-gap at 400 Pascal still has a lower thermal conductivity than Kapton, this limits the heat-flow out of the compressor and causes a long cycle time, see Figure 3.13. This long cycle time affects the average mass-flow of the compressor cell, resulting in this compressor cell having a lower average mass-flow than configuration 1.

Taking all these points into account, configuration 2 and configuration 3 are not viable to be used as compressor cell design in the compressor systems for the METIS cooler because of their inefficiency. They require too much input power for the amount of mass they can deliver. Configuration 1 has potential, but still has to be optimized for the use in the compressor systems of the METIS cooler.

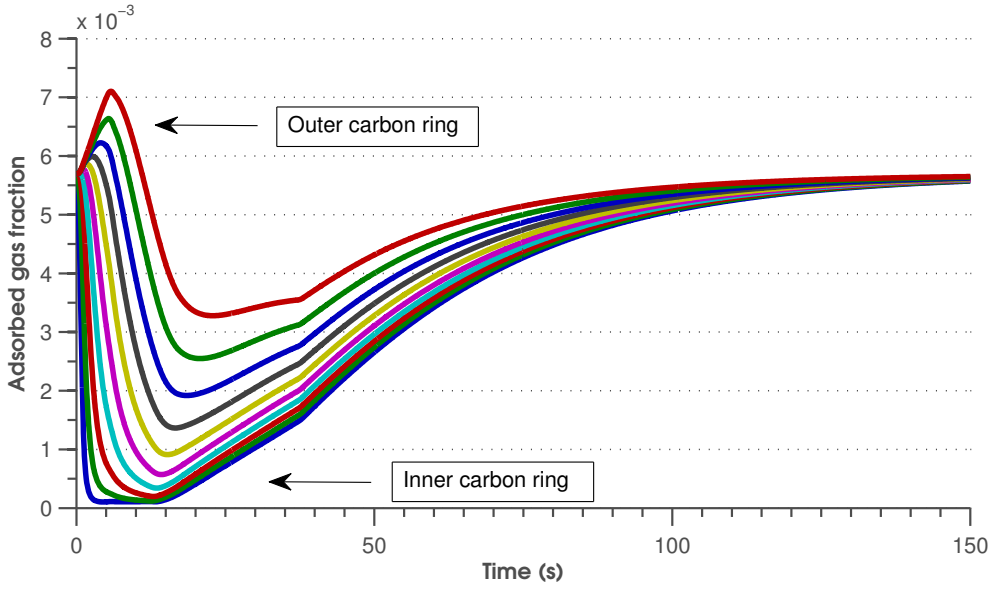

Figure 3.9: Adsorption ratio's of the 10 simulated carbon rings during one simulation. During the first 10 seconds, the outer rings adsorb the gas that is desorbed by the inner rings. Since the outer rings have more carbon mass than the inner rings, a small change in their adsorption fraction has a large influence on the total adsorbed gas fraction.

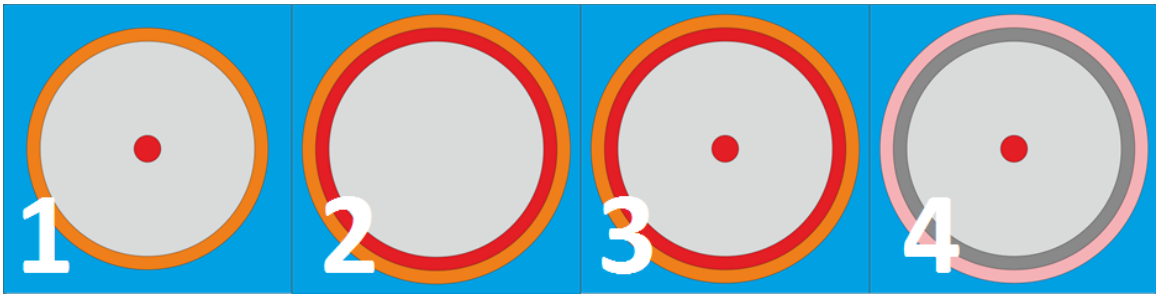

Figure 3.10: A schematic overview of the four simulated configurations.

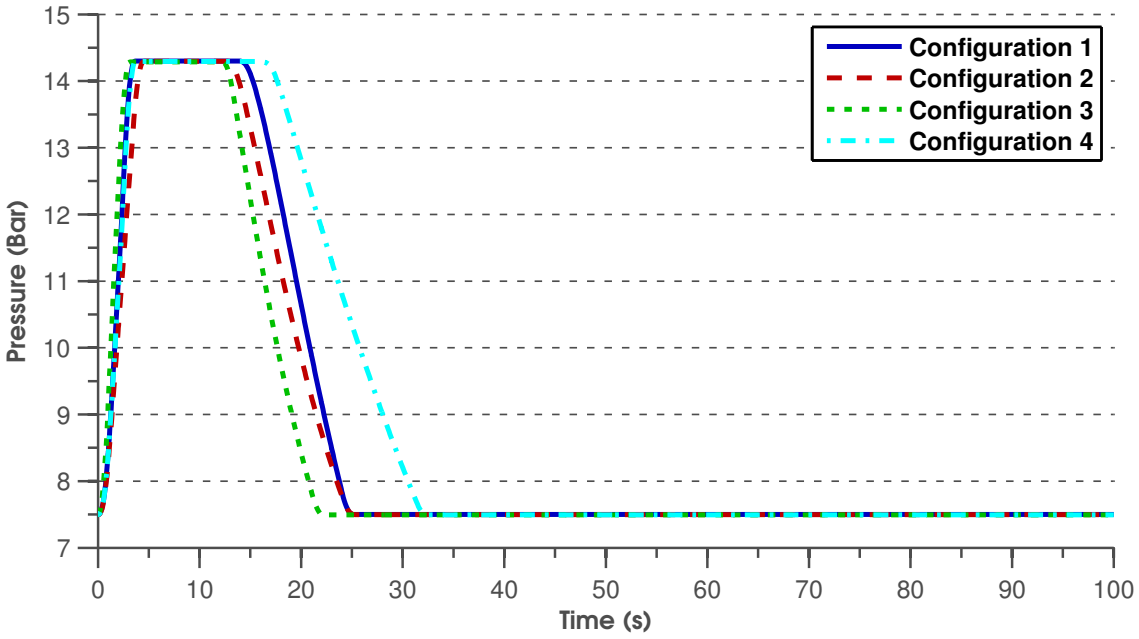

Figure 3.11: Build up pressure inside the compressors during one cycle. All compressors are able to reach the desired pressures and thus deliver mass-flow.

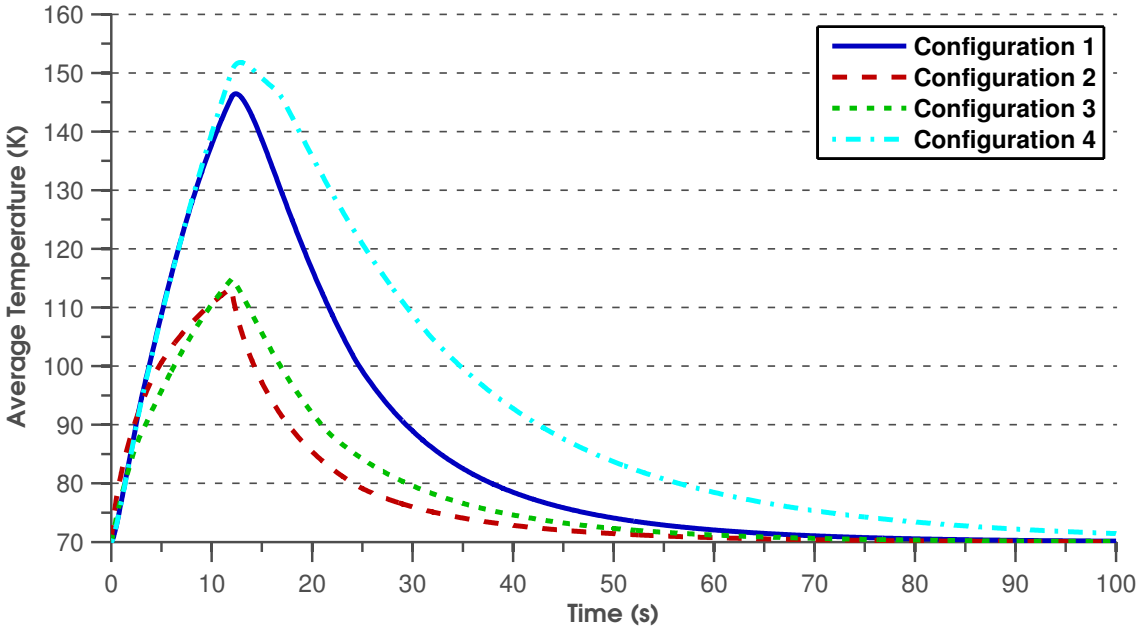

Figure 3.12: Average temperature of the carbon in the different compressors during one cycle.

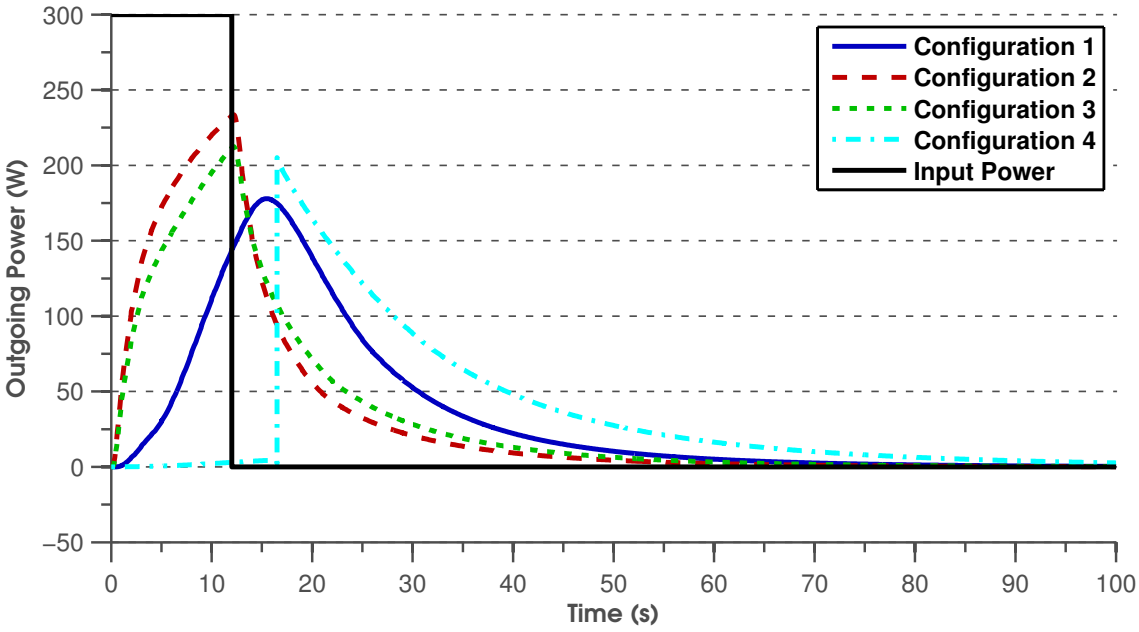

Figure 3.13: The power of the heat flowing into the heat sink during one cycle. The input power in all configurations is 300 W during the first 12 seconds.

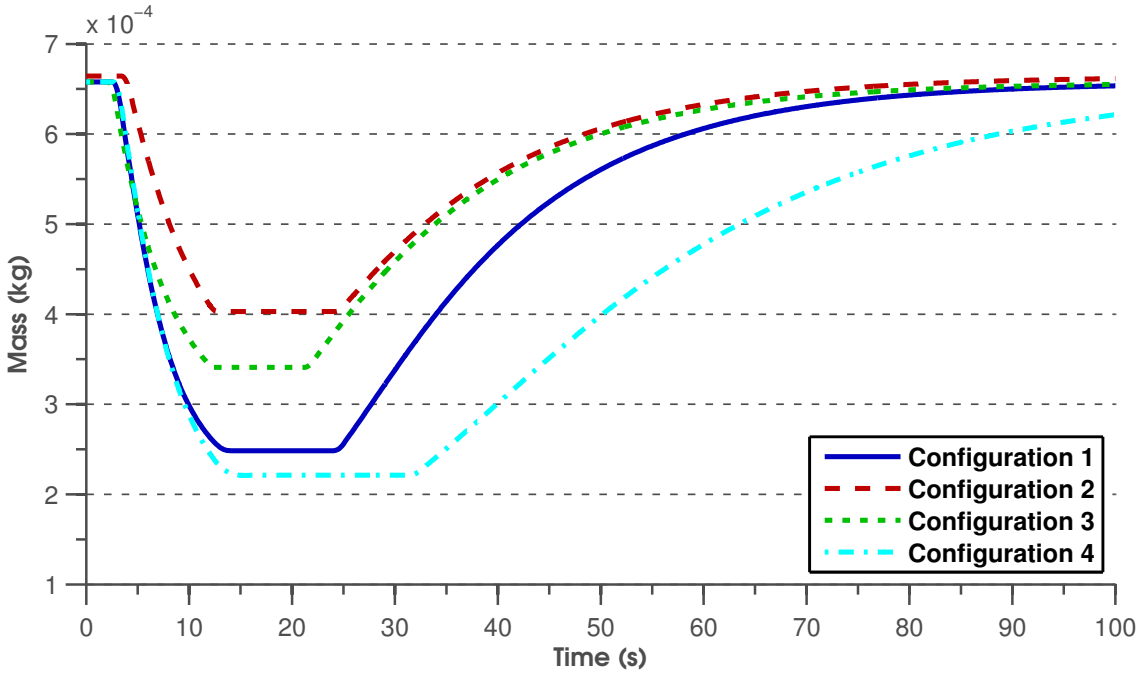

Figure 3.14: Helium mass inside a 1 meter long sorption compressor cell during one cycle. A larger mass different during the cycle means a larger amount of gas the compressor can deliver.

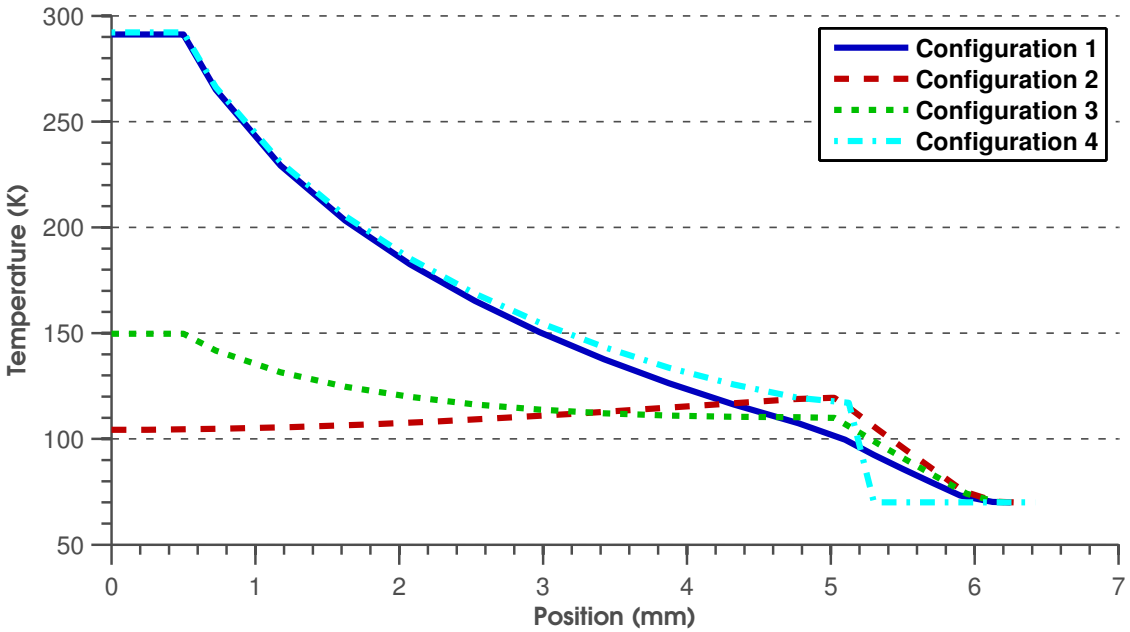

Figure 3.15: The temperature profiles in the sorption compressors as a function of the distance from the axis at the end of the heating phase.

3.3 Adding metal film

A temperature gradient over the carbon during heating reduces the performance of the compressor cell. This gradient over the carbon allows gas that is desorbed at the warm part of the compressor to be adsorbed in the cold part of the compressor.
A method is explored that might reduce this thermal gradient by increasing the effective thermal conductivity of the carbon. This will be achieved by adding a thin metal film between the cylindrical carbon pills. These metal films have a high thermal conductivity and should increase the total thermal conductivity in the radial direction.

Creating and simulating a two dimensional thermal problem in Matlab was expected not to be realistic in the current time frame. For this reason, a simple two dimensional model is created in COMSOL to simulate the effect of adding thin metal films between the carbon pills. Only a thermal simulation is performed with the model in COMSOL. The corresponding pressure and the amount of mass delivered are calculated using from the resulting temperature maps by using the method described in subsection 3.1.4.

In this simulation a few assumptions are taken:
- There is no heat of adsorption.
- There is no heat by the change in pressure.
- The working gas is helium.

Because of these assumption, only quantitative insight is expected on how the compressor will behave by adding thin metal films between the carbon pills.

Figure 3.16 illustrates the geometry of the simulated carbon pill and the added metal film. It is an axial symmetric simulation; the actual shape is a cylinder. The carbon pills have a radius of 7.5 mm and are surrounded by a layer of insulation of 1 mm. The inner radius of the metal film is fixed at 0.75 mm from the middle of the compressor. It is unlikely the thin metal film is always in perfect contact with the heater, for that reason a small space between the heater and the film is left open. This space counts towards extra void volume and is filled with helium.
The outer radius and the thickness of the metal film are varied. A small outer radius of the film forms a large gap between the film and the insulation, this gap is also filled with helium and counts towards extra void volume.
Increasing the thickness of the metal film will decrease the radial thermal resistance, but will also increase the heat capacity of the film, the volumes of the two gaps and the length of the compressor. If the input power density of the heater is fixed at 300 W/m, a longer cell means an increase in input power.

The metal film itself is made from aluminium. Aluminium has a good thermal conductivity, yet a low heat capacity. The low heat capacity of the aluminium film doesn't cause a significant change in the total heat capacity of the compressor.

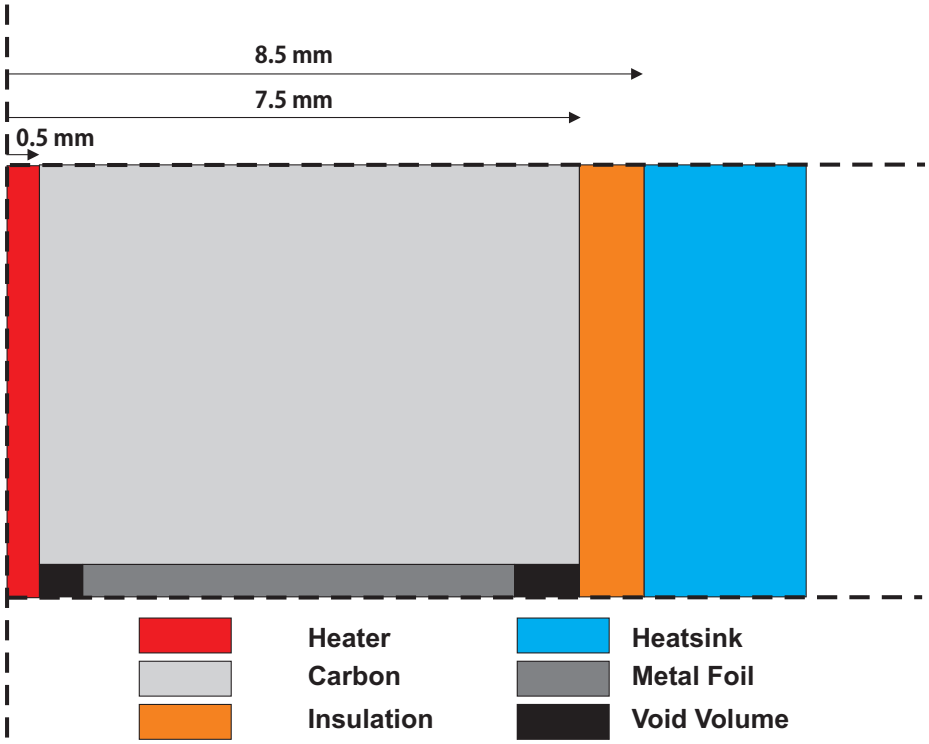

Figure 3.16: A schematic overview of the axial symmetrical geometry of the compressor that is used in the simulations in COMSOL. Because of the symmetry, this figure only shows half a carbon pill and a half metal sheet.

Representing temperature maps of a compressor with and without an aluminium film are presented in Figure 3.17. The maximum temperature near the heater is decreased significantly by adding the film. The heat can be distributed faster over the carbon, resulting in a lower the thermal gradient over the carbon.

Using the model in COMSOL, a parametric sweep over four different film thicknesses and four different outer radii is performed and the results are promising. In Figures 3.18, 3.19, 3.20 and 3.21 the total gas mass in the simulated compressor piece is presented for the different films thicknesses and outer radii during one cycle. In the legends of these figures the mass-flow and input power of the simulated compressors are indexed to the average mass-flow and average input power of a compressor without a metal film (index at 100). These figures illustrate, that by adding metal film between the carbon pills, the cycle time is affected to most. In most cases, only a slight increase in total mass delivered per cycle is realized. Since a compressor cell with added aluminium foil can cycle faster and deliver the same amount of mass per cycle, less compressor cells will be required in a compressor system. On the other hand, since the input power per cycle is fixed, this decrease in cycle time also causes an increase in the average input power of a compressor cell.

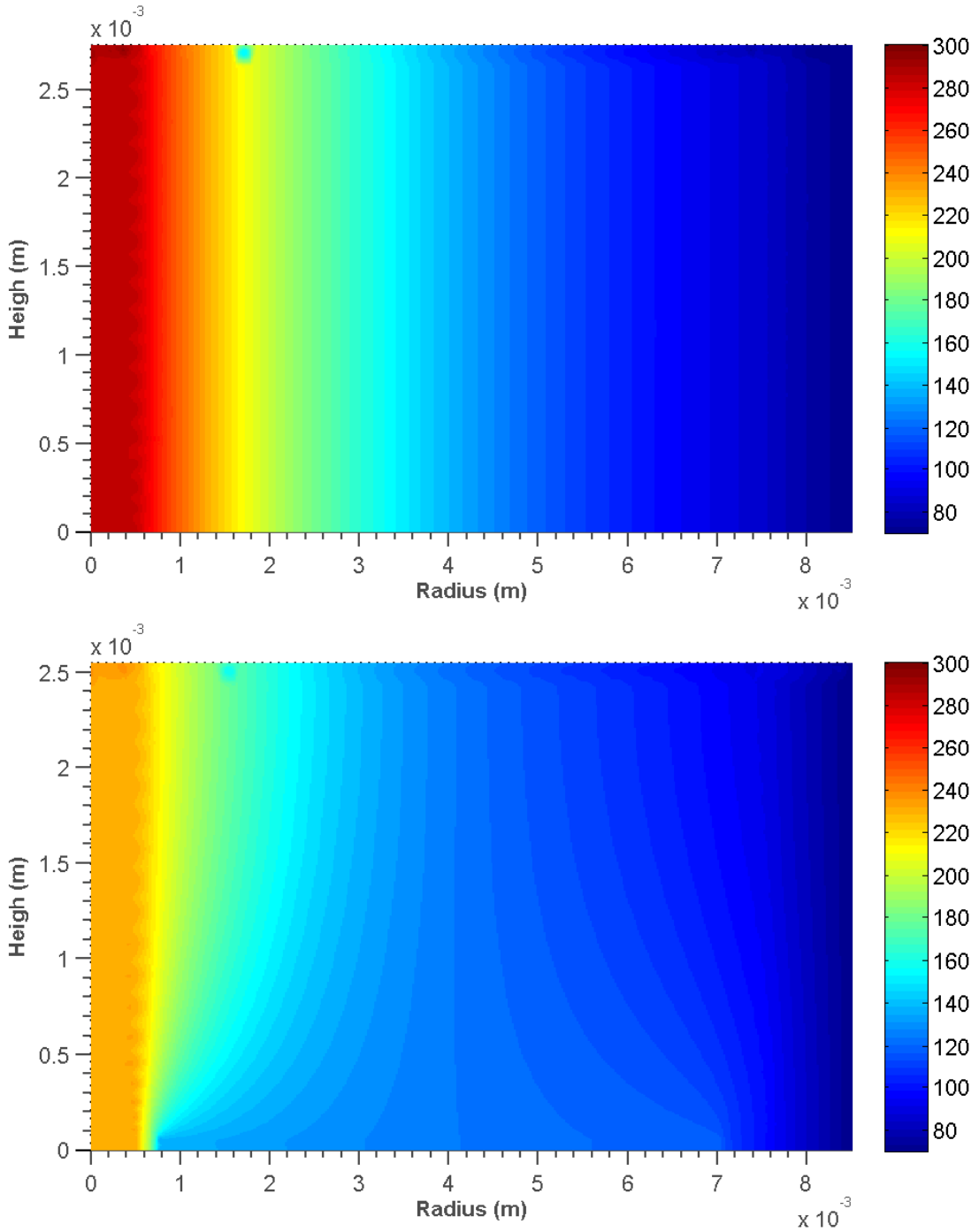

Figure 3.17: Thermal maps of a carbon pill without a metal foil (top) and with a metal foil (bottom) after 12 seconds of heating. Because of the symmetry only half a pill and half a metal sheet are shown. A few small artifacts appeared during the meshing process, these did not influence the simulation results.

Adding the aluminium film causes almost no change in the performance described by Equation 3.24, but the increase in mass-flow per cell lowers the total amount of compressor cells needed per compressor system. One of the best results, a compromise between the increase in mass-flow and the increase in input power, is achieved with adding aluminium foil with an outer radius of 6 mm and a thickness of 40 μm, see Figure 3.20. Here the mass-flow per compressor cell is increased 24%, which allows a decrease in total compressor cells of approximately 20%. For the helium stage this would mean going from 40 compressor cells to 32 compressor cells. For the other stages, a decrease in compressor cells with 20% only means a decrease of one or two cells. Since the average input power scales approximately with the increase in average mass-flow of a compressor cell, the input power per cell will increase. However, less compressor cells are needed per compressor system, which results to no change in input power for the whole compressor system.

Adding metal foil between the carbon pills will decrease the number of compressor cells and thus lower the production costs of the compressor systems and the space they take up, while leaving the input power unchanged

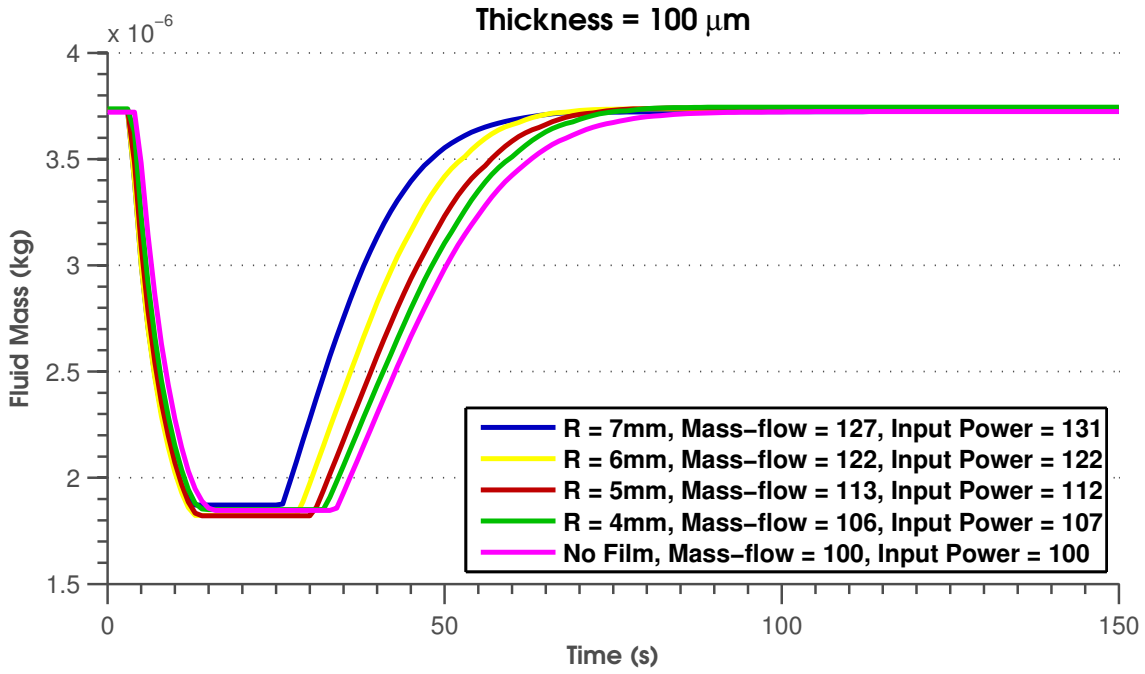

Figure 3.18: Helium mass in the compressor section as a function of time using a film with a thickness of 100 μm

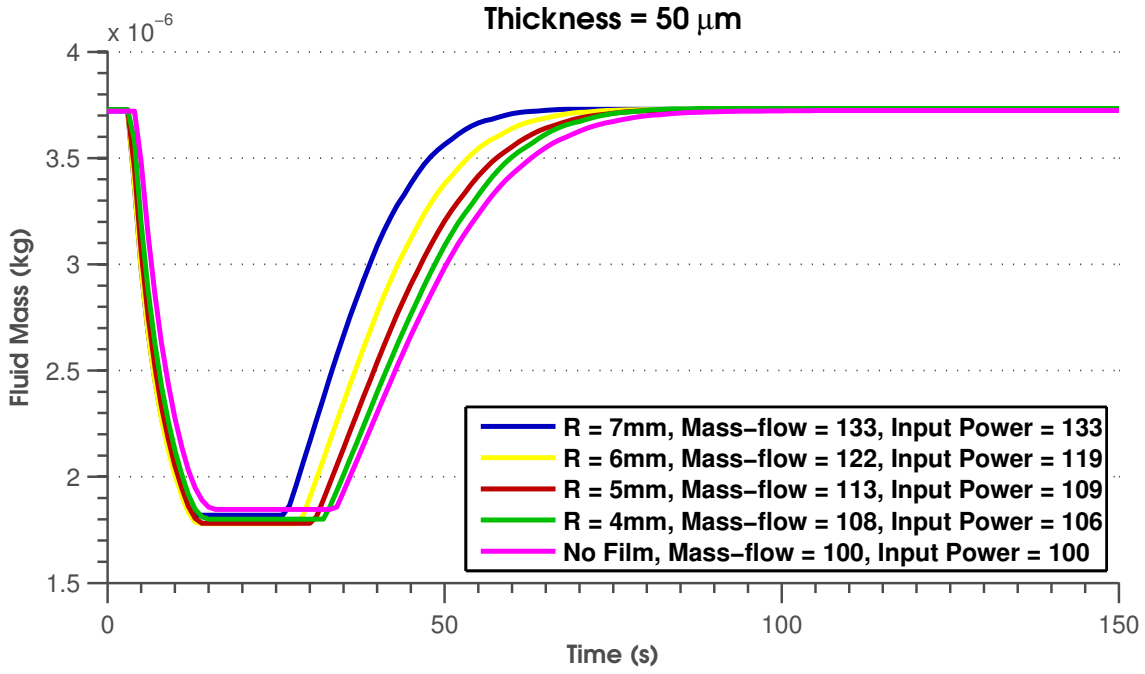

Figure 3.19: Helium mass in the compressor section as a function of time using a film with a thickness of 50 μm

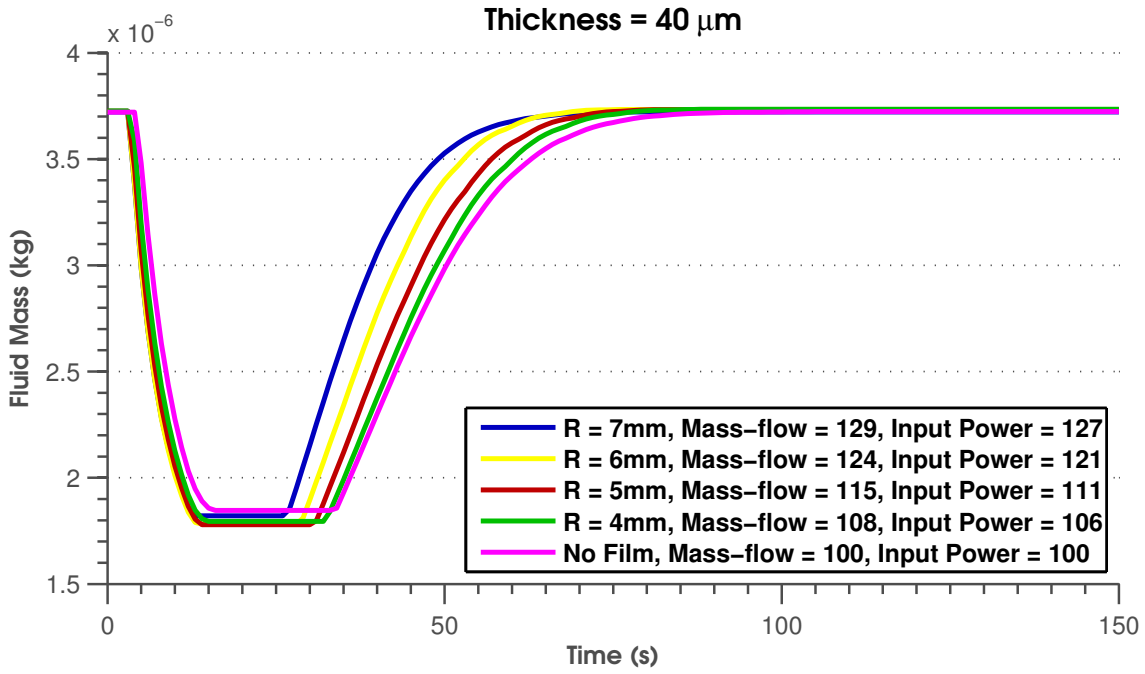

Figure 3.20: Helium mass in the compressor section as a function of time using a film with a thickness of 40 μm

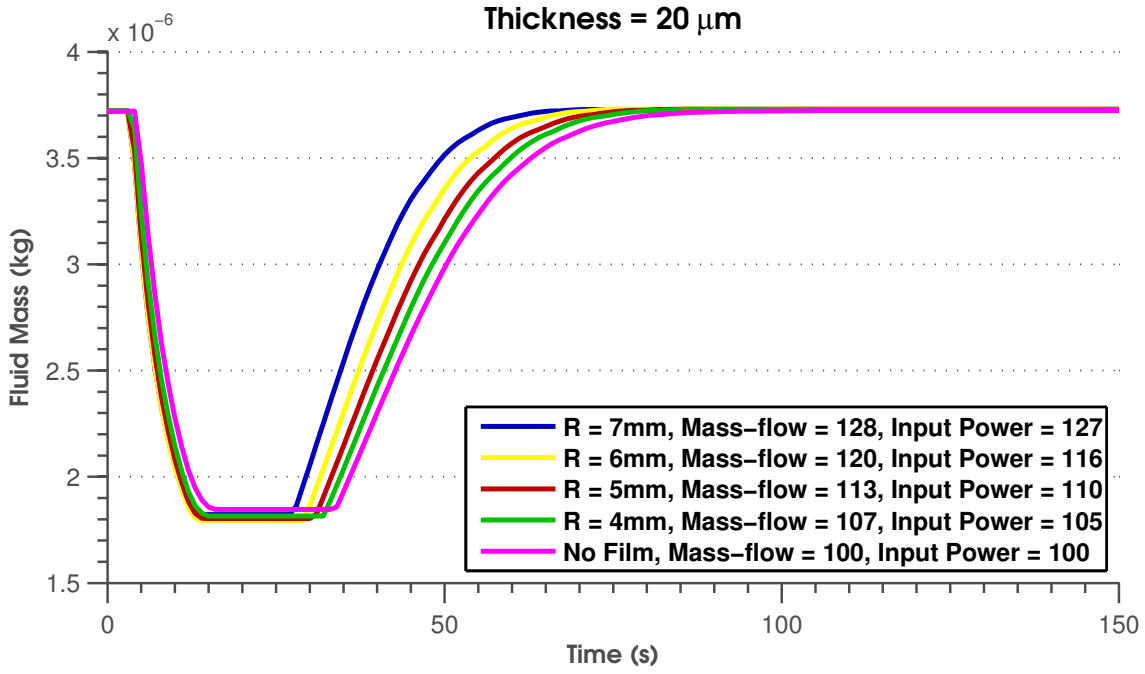

Figure 3.21: Helium mass in the compressor section as a function of time using a film with a thickness of 20 μm

4 Validation

Two models are developed to simulate a compressor cell; the first model only builds up pressure and does not allow mass-flow, the second model does allow mass-flow and is used for the evaluation of possible configurations, discussed in Chapter 2, and the design of the compressor systems for the METIS cooler, discussed in Chapter 5. For both models an experiment is designed to validate their results. In these experiments a sorption compressor is operated, while the resulting pressure and mass-flow are measured. This data is compared to the simulation results in order to confirm the validity of the model. Only a small selection of measured data is presented in this chapter, this selection is considered representative for all measured data.

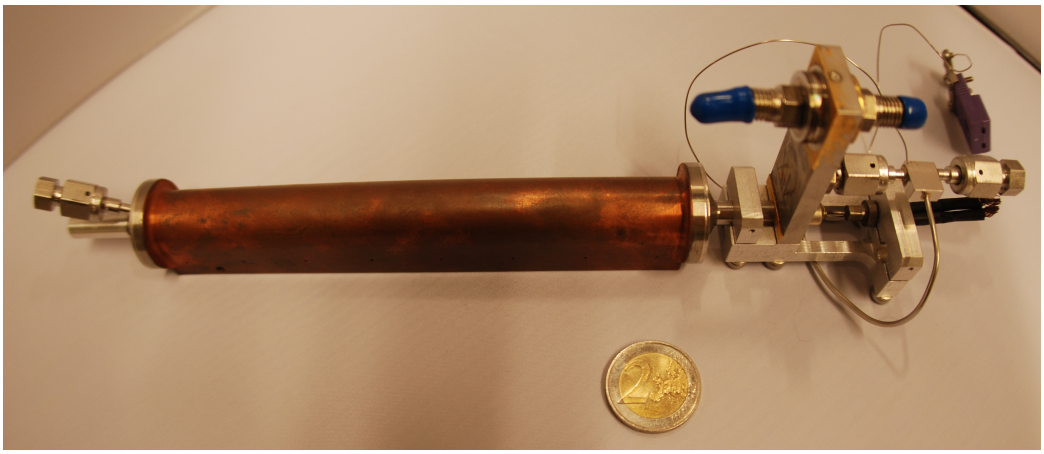

Figure 4.1: A photograph of an assembled sorption compressor. This is a slightly larger compressor than the one used in the experiments.

4.1 Sorption Compressor Cell

A sorption compressor cell with a gas-gap heat switch is used in the experiments. This is because no prototype sorption compressors with an insulation layer was available at the time of measurement. A photograph of a sorption compressor is presented in Figure 4.1. The compressor that is used in the experiments is 10 cm long and is rated at a maximum heating power of 30 W. To mimic the behavior of an insulation layer, the gas-gap is filled with helium gas at a constant pressure. The filling pressure of the gas-gap is 10 mBar, with this pressure the thermal resistance of the helium and the container resembles the thermal resistance of a typical Kapton insulation layer. The carbon pills inside this compressor have a diameter of 10 mm, a photo of two typical carbon pills is presented in Figure 4.2. They are placed inside a container with a wall thickness of 0.25 mm. The gap between the container and the heat sink has a width of 0.1 mm. The carbon pills on both ends of the container have an alternate

shape to fit inside the container. Because the shape of these carbon pills and the their position at both ends of the container, their behavior is expected to differ slightly from the simulation. A photograph of the container and the heat sink structure is presented in Figure 4.3.

To limit the radiation, outer surface of the container and the inner surface of the heat sink are gold plated. It is not known if the width of the gap is uniform or if the container touches the heat sink at any point. This might result into extra parasitic thermal conduction towards the heat sink.

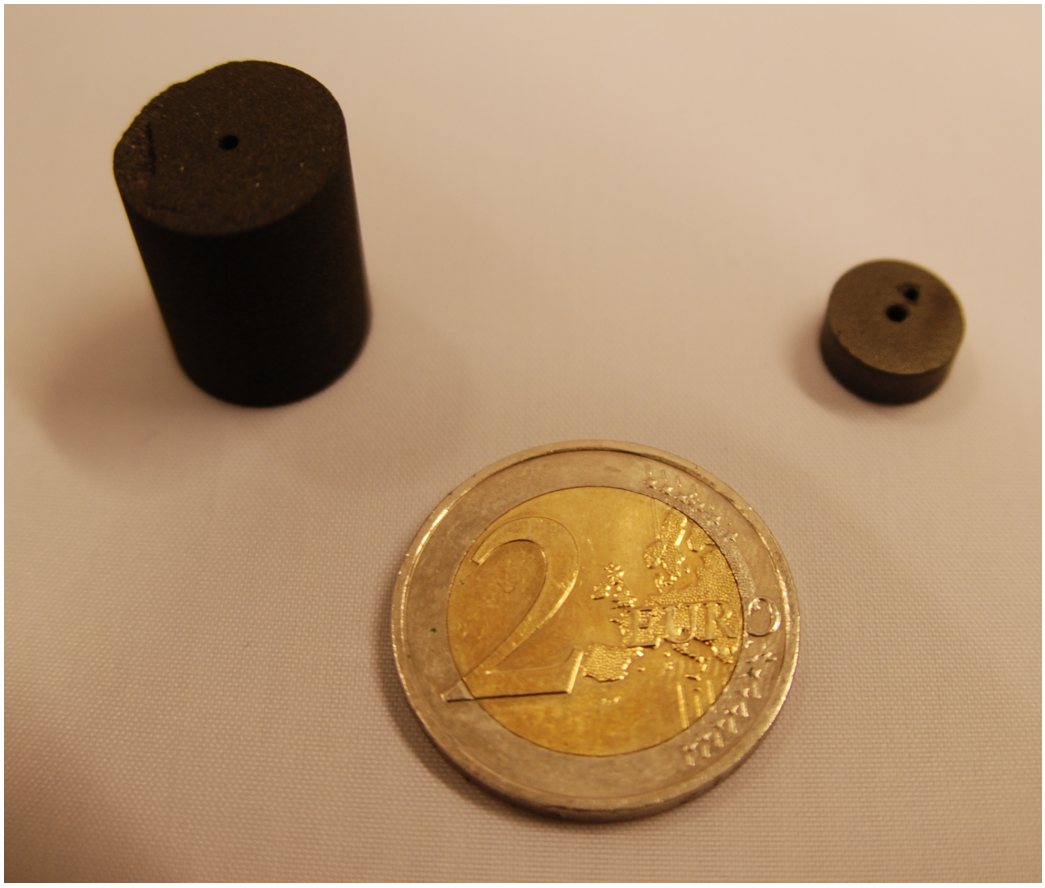

Figure 4.2: A photograph of two types of carbon pills. The carbon pill on the right has a small hole in it, this reduces the pressure drop inside the compressor.

Figure 4.3: A photograph of the carbon inside a container and the corresponding heat sink.

4.2 Experimental Setups

Of the two setups, the setup to validate the first model is the most simple setup. A schematic overview of this setup is presented in Figure 4.4. A vacuum pump is attached to the setup, removing all gas from the system before and (sometimes) in between measurements. The compressor is filled from a bottle of helium or neon gas. The filling pressure is set between 4 and 10 Bar, depending on the gas and the pressure restrictions of the different components in the setup. All valves will be closed after the compressor is filled to the desired pressure. During operation, a pressure sensor measures the pressure in the compressor, which is later compared to the simulated pressure.

The setup to validate the second model is a bit more complicated. To make this setup, two check valves (#9-10), two mass-flow meters (#11-12) and a relief valve (#13) are added to the first setup. The check valves allow the gas to flow into and out of the compressor at preset pressures. The filling pressure is set between 7 and 10 Bar, depending on the desired mass-flow and the limitations of the mass-flow meter. The relief valve is set to open at a pressure of 14.5 Bar. After the compressor delivers mass-flow, the redundant gas is vented into the laboratory. In this setup only helium is used.

The different components of the setup are mounted onto an aluminium plate that is positioned in a bath of liquid nitrogen. This aluminium plate acts as a heat sink, keeping the compressor at 77K. In Figure 4.5 photographs of compressor cells with the connected gas lines and valves are presented and the different parts are highlighted.

Tubing, the pressure sensor and the check valves add extra void volume to the compressor. For a realistic simulation result, the model takes this void volume into account. The exact method of determining the void volume is explained in Section 4.3. The heater is controlled via a Labview application. During measurements, the current through the heater is determined by measuring the voltage over a small calibrated resistance connected in series with the heater.

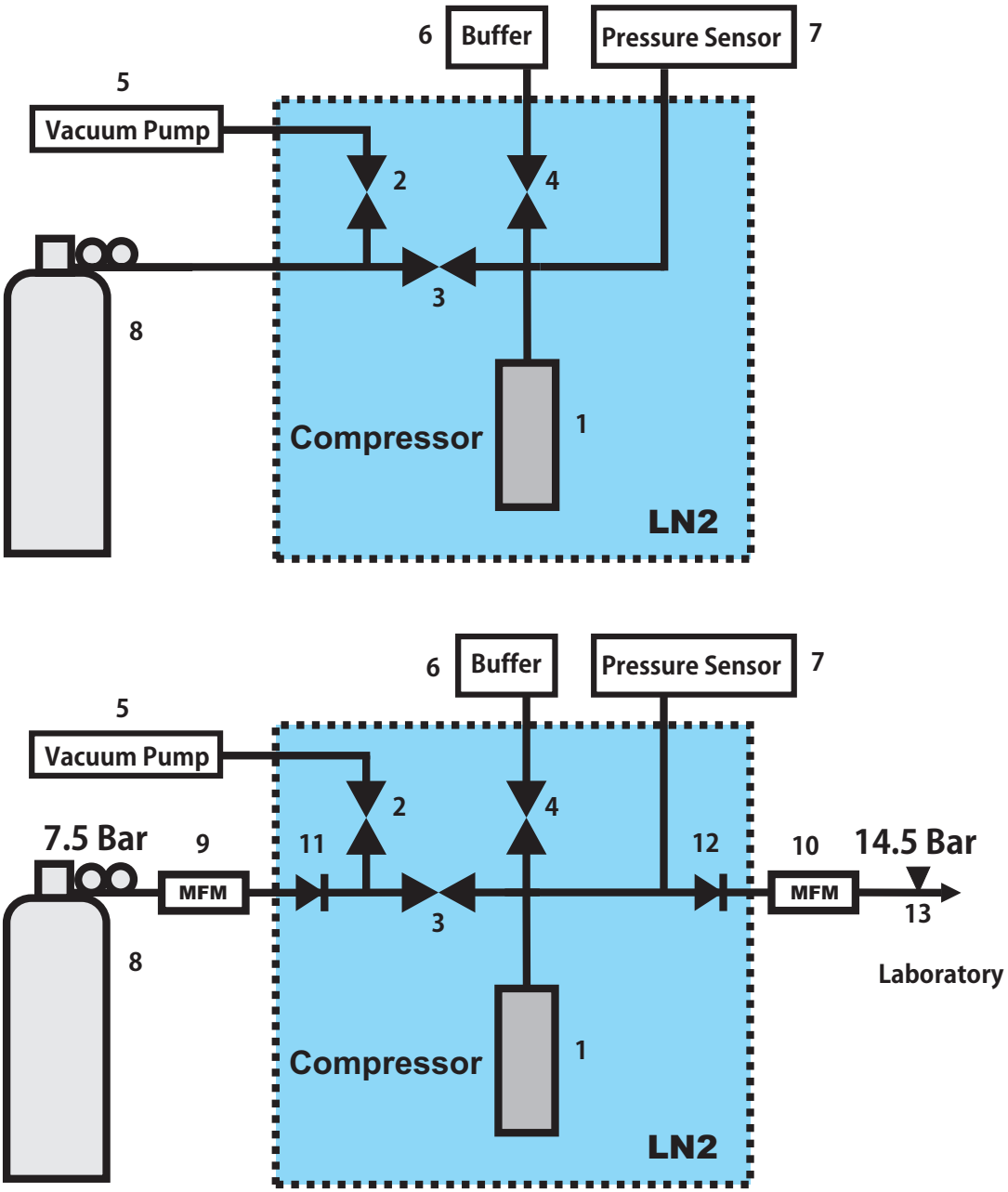

1	Compressor Cell	8	Gas Bottle
2-4	Valves	9-10	Mass-Flow Meters
5	Vacuum Pump	11-12	Check Valves
6	Buffer Volume	13	Relief Valve
7	Pressure Sensor		

Figure 4.4: Schematic overview of the first setup (top) and the second setup (bottom). The different components in the setups are numbered.

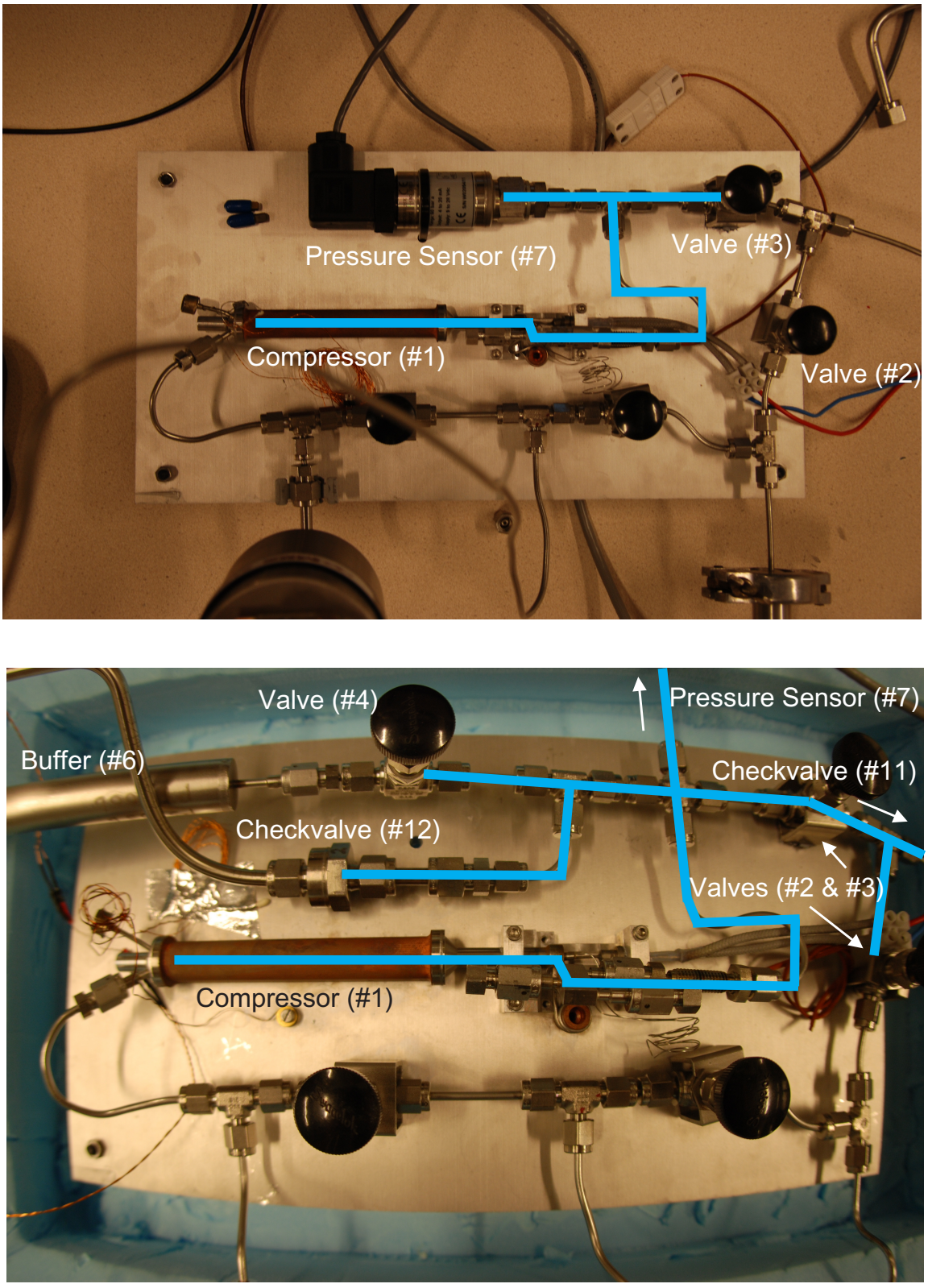

Figure 4.5: Photograph of setup 1 without the container and the buffer (top) and a photograph of setup 2 (bottom). The main components in the setup are labeled and the void volume is indicated in blue.

4.3 Void Volume

To compare the measured data and the results from the simulation, the model has to be corrected for the extra void volume in the experimental setup. The void volume in the setup consists of the volume in the tubing, the volume in the pressure sensor and the small volumes in the valves. To determine this volume a buffer with a known volume is added to the setup. A vacuum pump removes all gas from the setup and the buffer. The valve between the buffer and the compressor will be closed after all gas is removed. The compressor is then filled with helium while the heater keeps the carbon temperature well above room temperature. At these temperatures the adsorption of helium onto the carbon is very small and will hardly influence the determination of the void volume. The valve between the compressor and the buffer is opened when the desired filling pressure is reached. Opening this valve allows the gas in the setup to flow into the buffer volume, resulting in a decrease of the pressure. The total volume in the setup is calculated, by measuring the initial and final pressures:

$$P_i V_{setup} = P_f (V_{setup} + V_{buffer}) \tag{4.1}$$

Which can be rewritten as:

$$V_{setup} = V_{buffer} * \frac{P_f}{P_i - P_f} \tag{4.2}$$

Here P_i is the initial pressure and P_f is the final pressure after the valve between the gas lines and the buffer has been opened.

The measurements are performed using different filling pressures to make sure the residual adsorbed helium has no influence on the calculation of void volume. At higher filling pressures the measurement inaccuracy can consists of a small amount of residual adsorbed helium that is desorbed once the valve opens. At lower filling pressure the accuracy relies mostly on the accuracy of the pressure sensor.

For both setups the void volume is calculated and the results are presented in table 4.1. In this table an offset correction for the pressure sensor of -0.10 Bar is applied for the pressure measured in setup 1 and and an offset correction of -0.16 Bar is applied for the pressure measured in setup 2. The error in the pressure measurement, $\pm$ 0.04 Bar, is caused by static noise. This small error in the measured pressure leads to large errors in the calculated void volume if small filling pressure are used.
The carbon inside the compressor cell has a volume of 7.78 cc. Correcting for the porosity of 0.5 and the volume of the heater, the void volume in the carbon comes to a volume of 3.89 cc. This volume is subtracted from the total void volume to get the extra void volume added by the tubing and other components in the setup.

Measurements using larger filling pressures produced reliable and accurate results, for this reason the calculated void volumes by using a filling pressure of 15 Bar are used. This results in a total void volume in setup 1 of 5.76 $\pm$ 0.13 cc, which leads to an extra volume of 1.87 $\pm$ 0.13 cc and a total void volume in setup 2 of 5.89 $\pm$ 0.13 cc, which leads to an extra void volume of 2.00 $\pm$ 0.13 cc. A correction in the simulations is made for the extra void volumes in the setup.

Filling Pressure (Bar)	*End Pressure (Bar)*	Total Void Volume (cc)	Extra Void Volume
Setup 1:			
5.18 ± 0.04	0.67 ± 0.04	5.68 ± 0.39	1.79 ± 0.39
10.13 ± 0.04	1.33 ± 0.04	5.75 ± 0.20	1.86 ± 0.20
15.16 ± 0.04	2.00 ± 0.04	5.76 ± 0.13	1.87 ± 0.13
Setup 2:			
5.15 ± 0.04	0.70 ± 0.04	5.94 ± 0.39	2.05 ± 0.39
8.16 ± 0.04	1.10 ± 0.04	5.88 ± 0.25	1.99 ± 0.25
10.14 ± 0.04	1.38 ± 0.04	5.95 ± 0.20	2.06 ± 0.20
12.19 ± 0.04	1.64 ± 0.04	5.87 ± 0.17	1.98 ± 0.17
15.18 ± 0.04	2.05 ± 0.04	5.89 ± 0.13	2.00 ± 0.13

Table 4.1: Void volume measurement results of both setups.

4.4 Measurement Results

4.4.1 Setup 1

In the first setup pressure is built up and measured. This is done with helium and neon gas for a variety of heating times and filling pressures.

Helium:
Typical measurement results using helium and the corresponding simulations are presented in Figure 4.6. In the top graph the measured pressure and the simulated pressure with a void volume correction are presented. At the start of the measurement and the simulation, the slopes of the pressure are quite similar. After 5 seconds a deviation occurs between the measurement and the simulation. The model is able to build up higher pressures and the decrease pressure during the cool down phase is initially slower than in the measurement. The void volume correction is already applied in these simulations. However, two other corrections have to be applied to make the simulation more realistic:

A correction for extra parasitic conductivity from the container to the heat sink.
The total thermal conductivity of the gas-gap is set from 56 mJ/Km to 70 mJ/Km. This affects the slope of the pressure during the cool down, still this change is barely noticeable in the simulation results.

A correction for the heat sink temperature.
The compressor is not entirely covered by liquid nitrogen. A part of it is exposed to the air in the laboratory. If the compressor is not perfectly attached to the aluminium plate, the temperature of the compressor might be slightly higher than 77K. With each measurement a small amount of the liquid nitrogen evaporates and the nitrogen level drops. The will increase the effective heat sink temperature during each of the following measurements. The temperature of the heat sink in the model is set between 77K and 80K, depending on how many measurements have been performed after refilling the container with liquid nitrogen. Increasing the heat sink temperature will affect the amount of gas that is adsorbed to the carbon at the start of each cycle and how fast the compressor can cool down after heating.

In the bottom graph in Figure 4.6 all corrections are applied to the model. Now the resulting overall shape of the measured pressures does match the simulated pressures. The biggest difference between the simulated data and the measurements is expressed in the tail of the pressure. The pressure in the model is able to recover quicker to the initial pressure. Since this effect is more dramatic while heating longer, it is expected that this behavior is due to the temperature of the heat sink during the cool down of the compressor. If the temperature of the heat sink increases too much during a compression cycle, it can transport less heat away from the compressor, resulting in a longer recovery time.

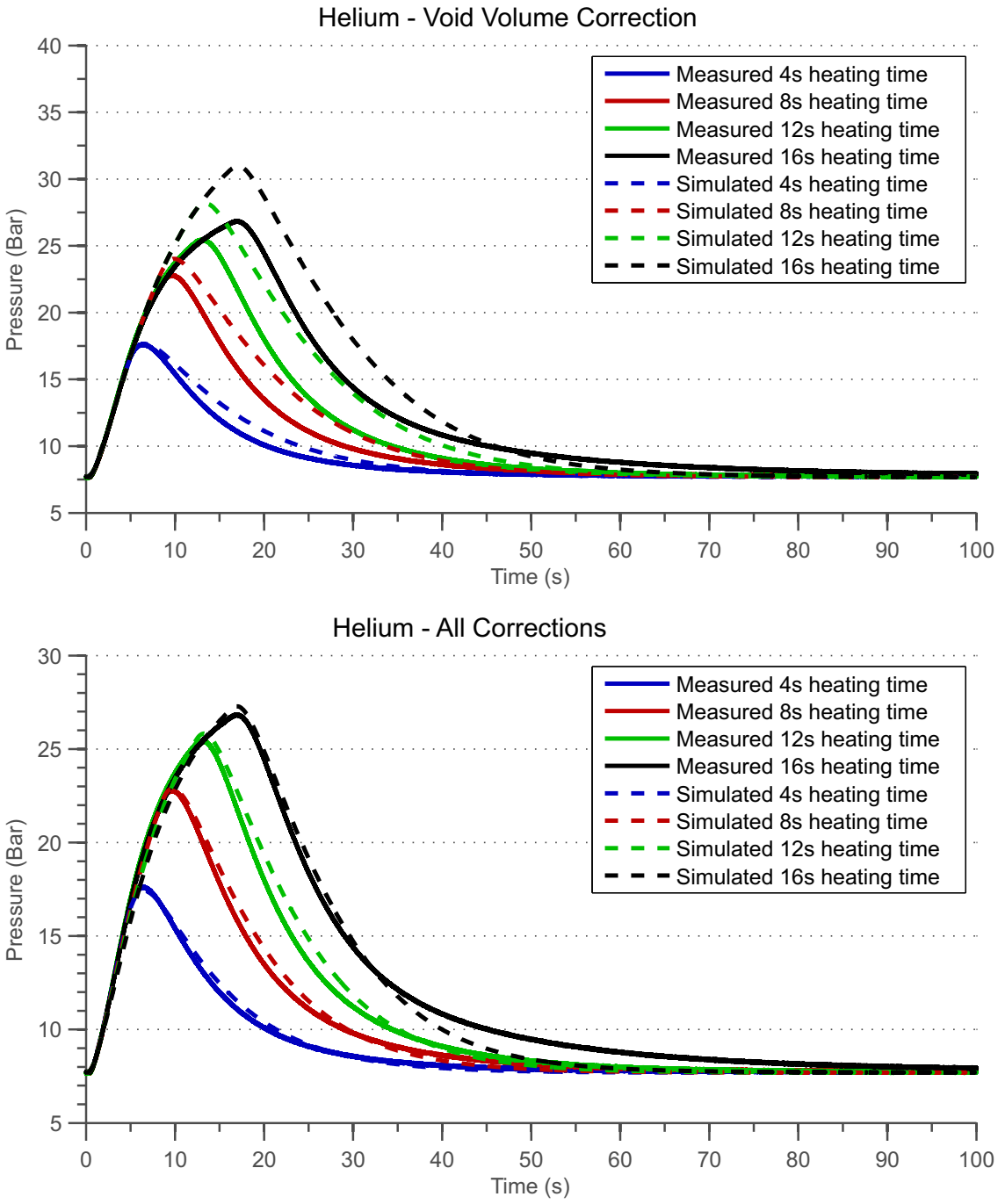

Figure 4.6: Measured helium pressure (solid lines) including the simulation results using only a void volume correction (top) and the simulation results including all corrections (bottom). The filling pressure of the compressor in these measurements is 7.7 Bar. Heat is generated for 4, 8, 12 and 16 seconds using 30 W of input power. The heat sink temperature in the simulation is set at 77, 78, 79 and 80K.

Neon:

More neon gas can be adsorbed onto the carbon compared to helium gas at a heat sink temperature of 77 K. For this reason slightly different operating conditions are used to prevent reaching a pressure that could damage components in the setup. The filling pressure is set around 5 Bar and measurements with up to 8 second of heating are performed. The same corrections that are applied in the simulations using helium, are also applied in the simulations using neon. Figure 4.7 presents typical the measurement results using neon as working gas and the corresponding simulations including all corrections. Here the overall shape of the simulated pressures also matches the measured pressure. Despite the unmatched tail of the pressure in the simulation using helium, the tail of pressure in the simulations using neon does match the measured pressure to a large extend. It is likely that this is caused by the lower heating time.

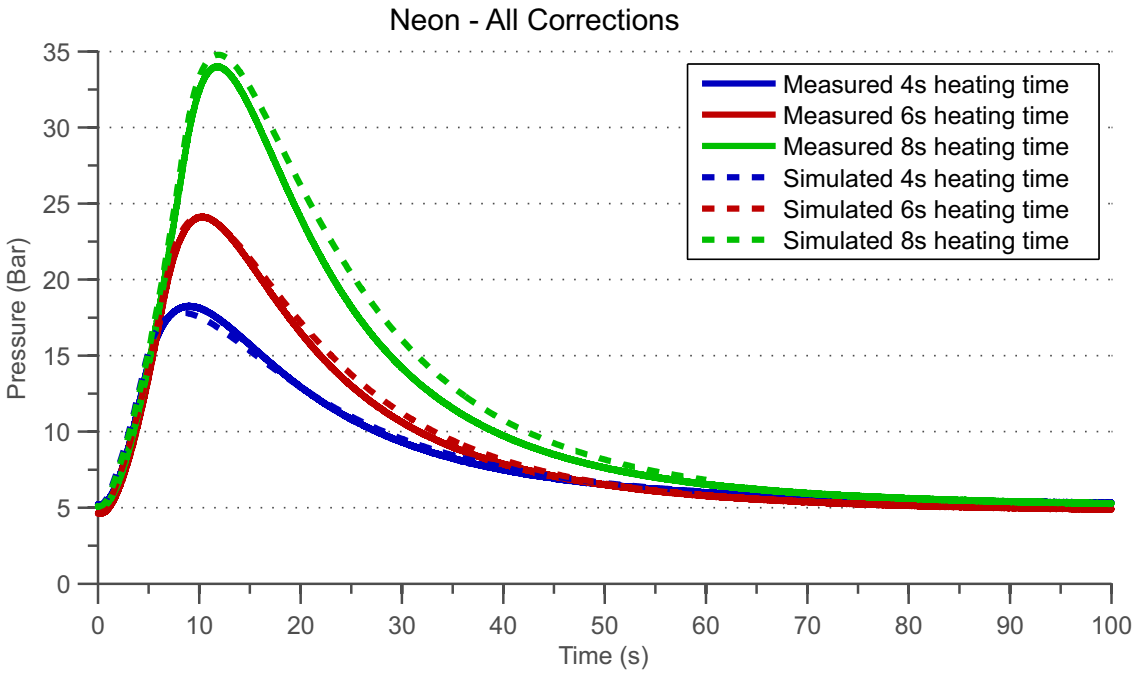

Figure 4.7: Measured neon pressure (solid lines) and the simulation results including all correction (striped).The filling pressures are 5.2 Bar, 4.9 Bar and 5.1 Bar for a heating time of 4, 6 and 8 seconds.

4.4.2 Setup 2

In the second setup mass-flow is enabled. The mass-flow is realized by adding two check valves (#9-10) and a relief valve (#13) to the first setup. The compressor cell is filled with helium from a gas bottle. Once the compressor establishes mass-flow, the redundant helium gas is vented to the laboratory.

During the first measurements, this setup did not perform as expected. A low amount of mass was delivered by the compressor cell, 0-30% compared to the simulation and the mass-flow into the compressor started when the pressure in the compressor was around 11 Bar. At this pressure the mass-flow into the compressor should not be able to start. By analyzing data from the measurements, we suspected the first check valve (Component #11 in Figure 4.4) to be leaking. This means that pressure is build up in the setup, but also in the volume before this check valve. Once the compressor starts to cool down again, the pressure in the compressor starts to drop. Since the volume before the check valve is at high pressure, the mass-flow into the compressor starts much earlier.
To test our hypothesis, a pressure sensor is placed temporarily between the first mass-flow-meter and the first check valve (Component #9 and #11see in Figure 4.4. Data from this pressure sensor validated our suspicion, the check valve was leaking and it then replaced by a functioning leak tight check valve.

After the replacement of the first check valve, the setup performed better. However, the compressor could still only deliver around 50-70% of the mass that was delivered by the simulated compressor. A peculiar bump in the mass-flow was measured during the operation of the compressor cell. The measured mass-flow including this bump is presented in Figure 4.8. This measurement is performed using

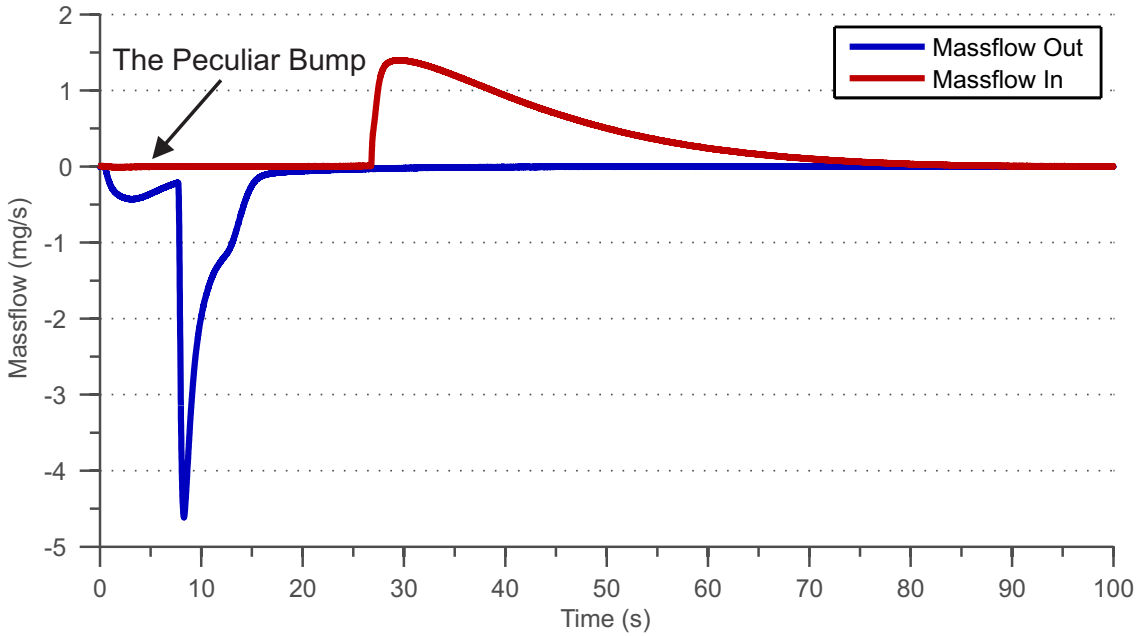

Figure 4.8: A typical measured mass-flow in the second setup including the peculiar bump.

helium at a filling pressure of 8 Bar and heating for 12 seconds.
The pressure in volume between the second check valve and the relief valve (components #12 and #13 in Figure 4.4) should always stay at 14.5 Bar. This bump in the mass-flow could indicate that gas is leaking out of this volume. When the compressor builds up pressure, this volume now has to be re-filled to a pressure of 14.5 Bar. During the pressurization of this volume, the mass-flow meter should register a small mass-flow just before the relief valve opens. To verify the leakage, a pressure sensor is placed temporarily between this second check valve and the relief valve. Data from this pressure sensor confirmed that gas was leaking out of the volume. To measure if this volume was leaking helium to the laboratory, a helium mass spectrometer is used to measure the levels of helium outside the setup. No high levels of helium gas are measured with the helium mass spectrometer, which means the leakage occurred internally via the check valve (Component #12). Before this check valve was placed in the setup it was tested at room temperature and at 77 K, during these tests it showed no signs of leakage. A possible explanation of the sudden leakage is the thermal gradient over the check valve. In this setup the check valves are not entirely covered by liquid nitrogen, which might create a thermal gradient over the valve leading to leakage. Removing the thermal gradient is achieved by heating up the check valve. The check valve is shielded from the liquid nitrogen using multilayer insulation (MLI) while heating it with a light bulb (unsuccessful) and a fan (successful), see Figure 4.9. After the thermal gradient was removed from the check valve, the setup showed no further problems.

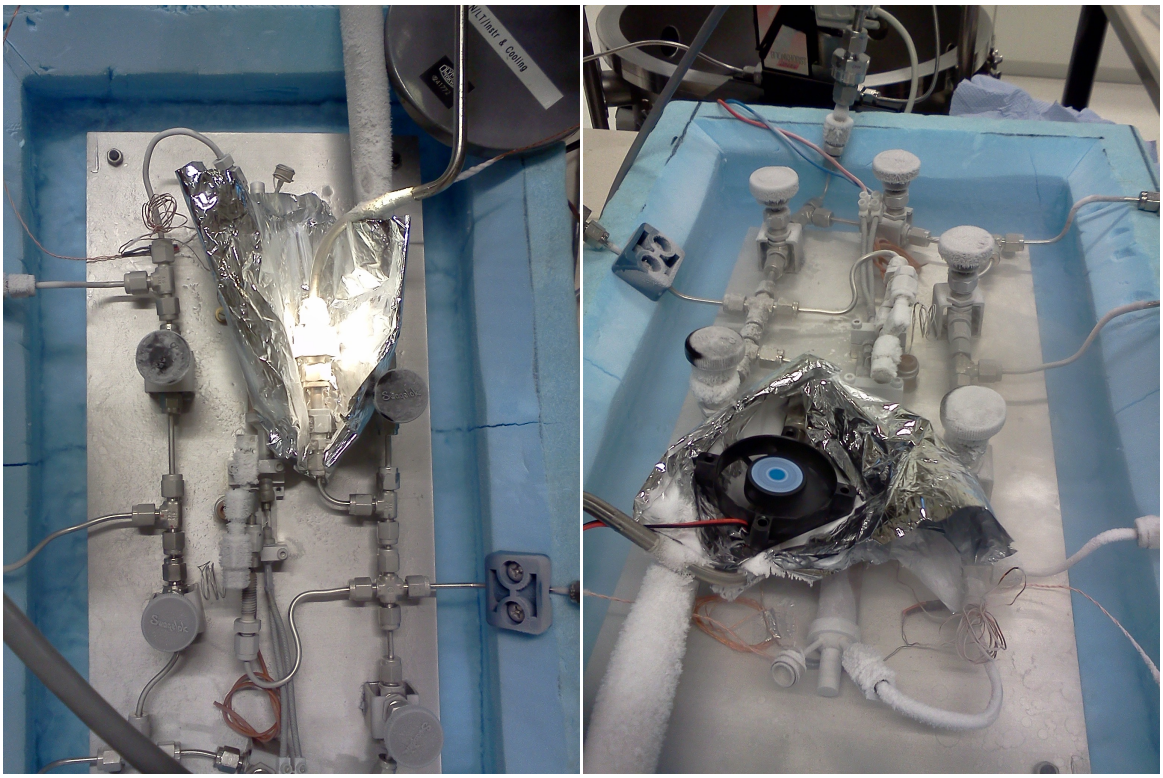

Figure 4.9: Using a light bulb and a fan to heat up the malfunctioning checkvalve.

Helium:
The mass-flow in the setup is measured by two mass-flow meters (#9 and #10). They measure the mass-flow at the inlet and at the outlet of the compressor. The measured pressure and mass-flow with the corresponding simulated data of a single cycle are presented in Figures 4.10 and 4.11. The mass-flow meter at the inlet of the compressor measures a small steady flow while gas is refilling the compressor and the mass-flow meter at the outlet measures a high flow for a short period. In Figure 4.11 the values for the mass-flow out of the compressor are negative because the gas leaves the compressor. The same type of corrections that are applied in the simulations for setup 1 are also applied to this simulation. Since this setup has more void volume, a larger void volume correction is applied. The measurement presented in these graphs is the first measurement after refilling the container with liquid nitrogen. For that reason the compressor itself is partly covered by liquid nitrogen and no correction for the heat sink temperature was necessary. The simulated pressure and simulated mass-flow are plotted in the same graph as the measured data. The simulation results match the measured data quite good. The simulated mass-flow starts slightly earlier than the measured mass-flow. This is directly related to the cracking pressure of the relief valve. The relief valve opens at 15 Bar and closes at 14.5 Bar, see Figure 4.10. This delays the start of the mass-flow for a small moment, but increases the peak flow when the valve opens. The simulated compressor cell is able to deliver a total amount mass of 35.2 ± 0.2 mg per cycle. The error in this value is caused by the error in the void volume and the error in the initial pressure. In the experiment, the compressor cell is able to deliver a total mass of 34.2 ± 0.7 mg per cycle. This value is derived by analyzing four measurements that use the same operational conditions. The amount of mass that is delivered in the measurements is slightly lower than the simulated value and can be explained by small differences in operating and geometric conditions.

Another measurement includes multiple cycles with a fixed time between the start of each cycle. The mass-flow of a measurement including four cycles is presented in Figure 4.12. The cycle time is set at 90 seconds per cycle. During each of these cycles the level of the liquid nitrogen drops slightly, reducing the amount of heat the liquid can effectively transfer away from the heat sink. In the measurements this results into a higher heat sink temperature at the end of each cycle and thus a lower amount of adsorbed helium at the start of the next cycle. In the graph this is best illustrated by a slight decrease in the measured peak flow of each cycle. This is also the reason why in the simulations a correction has to be made for the heat sink temperature. In the simulation of these four cycles, the value of the heat sink temperature is fixed. For this reason the simulated mass-flow does not drop each cycle, it stabilizes. A stabilized flow of 35.1 mg per cycle is found for the simulated compressor cell.

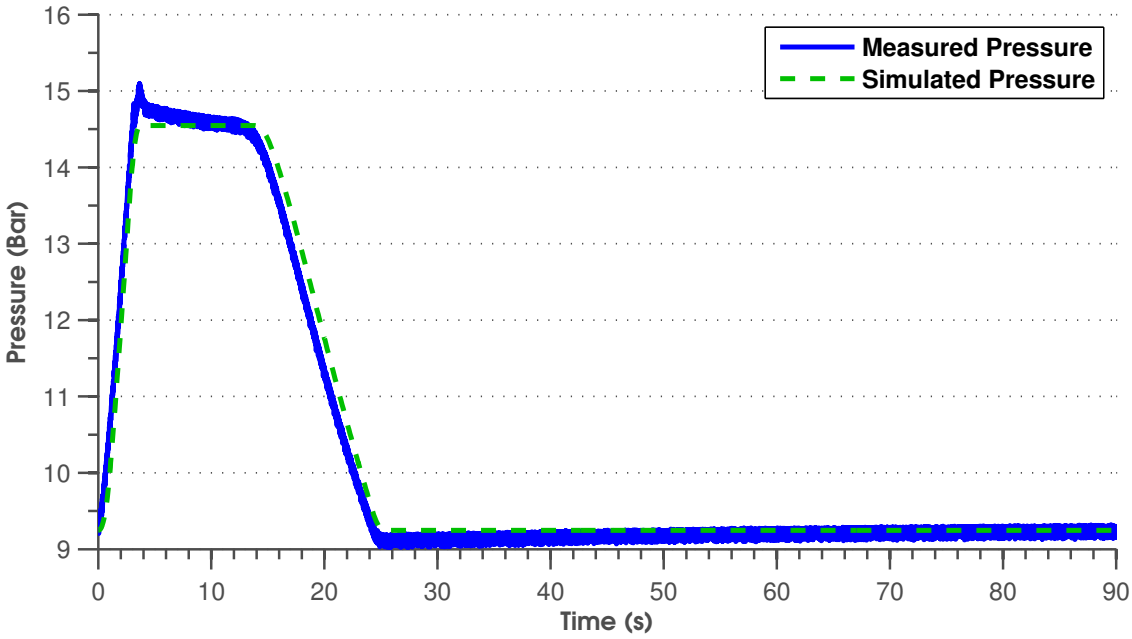

Figure 4.10: The pressure in the second setup for a single cycle, both measured (solid blue) and simulated (striped green). The filling pressure is 9.2 Bar and 30 W of heat is generated for 12 seconds.

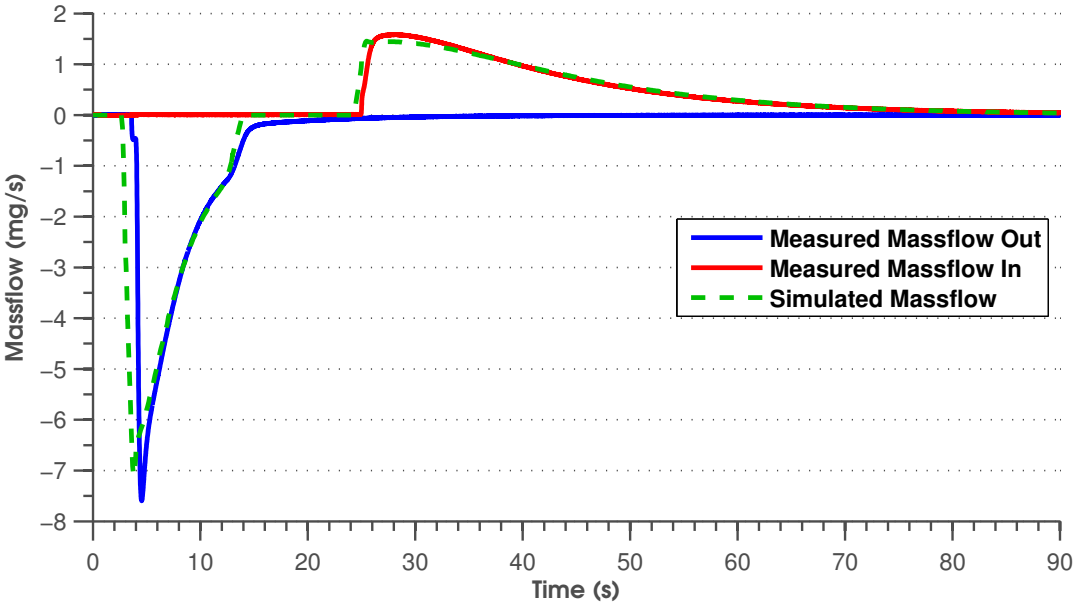

Figure 4.11: The mass-flow out of the compressor (solid blue), the mass-flow into the compressor (solid red) and the simulated mass-flow (striped green).The filling pressure is 9.2 Bar and 30 W of heat is generated for 12 seconds.

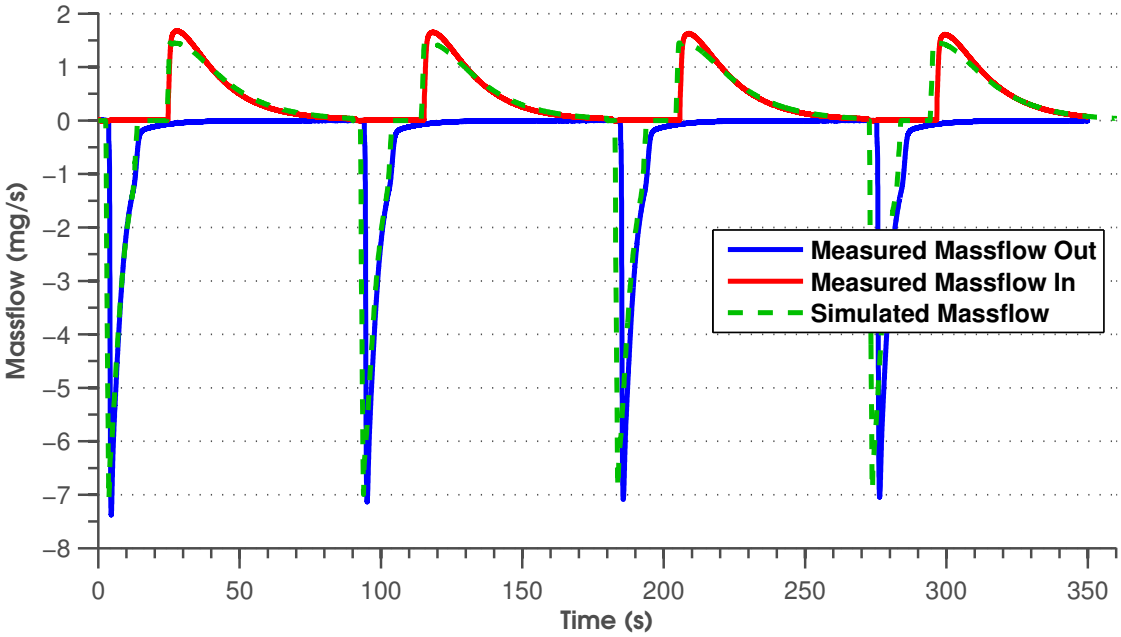

Figure 4.12: The mass-flow of four cycles in and out of the compressor. The mass-flow out of the compressor (solid blue), the mass-flow into the compressor (solid red) and the simulated mass-flow (striped green).The filling pressure is 9.2 Bar and 30 W of heat is generated for 12 seconds per cycle.

4.5 Discussion

Small differences in operating conditions between the model and the experiment, especially the heat sink temperature, can cause big differences in performance. To match the measurement perfectly, all operating conditions need to be known at all times. Since this was not the case in the basic experiments that were performed, the model was not able to match the measured pressure and mass-flow perfectly. Still, the model is able to match the measured data to a large extend; the overall shapes of the simulated pressure and mass-flow are very similar, the timing of all events occurs at almost the same time and the measured pressures and mass-flow are very close to the simulated values.

The compressor cell used in the experiment is only 10 cm long, the compressor cells for the METIS compressor will be 50 cm long. Because of its longer length, the METIS compressors will be less influenced by similar sized void volumes and small geometric differences between the compressor and the simulation.

In total, the measurement and simulations results show a very large overlap. For this reason it is safe to say that the model is validated. The model should be able to predict the performance of the compressor cells for the compressor systems in the METIS cooler, under the condition all operating parameters, especially the heat sink temperature, will be very close to the parameters in the model.

5 METIS Compressor Systems

In Chapter4 is explained that the dynamic thermal model has been validated and can be used to design the compressor systems for the METIS cooler. In Chapter 3 is explained that the best configuration without a gas-gap heat switch is *configuration 1*. This has the heater in the center of the carbon, which is surrounded by a layer of Kapton. The parameters in this configuration have to be optimized for the use in the different compressor systems in the METIS cooler. The goal of the optimization is to find a good compromise between the number of compressor cells in the compressor systems and the amount of input power these systems require. The details of the optimization and its results are discussed in this chapter.

5.1 Optimization Parameters

Finding the optimal parameter settings for the different compressor systems is achieved by performing a parametric sweep over a few selected parameters. For this sweep, three parameters are selected, two of them are geometric parameters; the diameter of the carbon pill and the thickness of the insulation layer. The third one is an operating parameter, which is the heating time. The mass-flow and pressure requirements of the different stages are fixed at the values derived in the statical analysis of the METIS cooler, as is shown in Table 1.2.

Heating time: From early analyses, it is proven that heating for short periods with a high power gives better results than heating for longer periods with a lower power. For this reason the heating power density with respect to the compressor length is fixed at 300 W/m, this is the maximum power density the heater is able to provide without causing degradation [23]. The heating time will determine the total amount of heat that will generated in the compressor per compression cycle.
If the heating time not long enough, it will only allow a small amount of gas to be desorbed from the carbon, resulting in no- or only a small amount of gas the compressor can deliver. This results in a large amount of compressor cells that deliver only a small amount of mass.
Heating while most of the gas is already desorbed will have a negative effect on the efficiency of a compressor cell. Also, it it will increase the cycle time and lower the average mass-flow per compressor cell, described by Equation 3.20. This results in a large amount of compressor cells that require a high input power. The optimum heating time is strongly dependent on the carbon pill diameter, the thickness of the insulation layer and sorption characteristics.

Carbon pill diameter: The diameter of the carbon pill influences the total volume of the carbon and thus total amount of gas that can be adsorbed and desorbed per cycle. The diameter of the carbon pill also influences the thermal resistance between the heater and the heat sink. Smaller diameters allow faster cycling and a higher average mass-flow per kilogram of carbon, while larger diameters are proven to be more efficient. The carbon pill diameter will be varied from 8 mm to a maximum of 17.5 mm, which is the largest pill diameter the supplier can produce.

Insulation thickness: The layer of insulation limits the heat losses during heating. Increasing the thickness of the insulation layer will increase the efficiency, but will also increase the cycle time of the compressor at the cost of a lower average mass-flow.

5.2 Optimization Results for the METIS compressor systems

In the optimization process the first focus was on the geometric parameters; the diameter of the carbon pill and the insulation thickness. A preliminary wide sweep over all parameters is performed. Using the resulting data, a pill diameter and insulation thickness are chosen. It was made sure that that chosen pill diameter and insulation thickness can provide both a low input power and a low number of cells, depending on the choice of heating time. An exact value for the heating time is determined by further optimizing the compressor cells. The optimization process for the heating time is presented in Figures 5.2 to 5.5. The cycle time of the different compressor systems as a function of the heating time is presented in Figure 5.1. For all compressor cells, dimensions are chosen to fit the same heat sink structure, making the manufacturing process easier. In table 5.1 an overview of the optimization results is provided. The number of cells, the input power and the cycle time of the system is determined by using the equations from Section 3.2.1 to 3.2.3.

Helium Compressor:
For the helium compressors a pill diameter of 15 mm and an insulation thickness 1.2 mm are chosen. This adds up to a total diameter of 17.4 mm. In the optimization of the heating time, the focus was primarily on the total input power of the system, see Figure 5.2. The optimization resulted in a heating time of 11.8 seconds. The helium compressor system requires 40 compressor cells and 625 W input power using this heating time. Each compressor in this system has a cycle time of 112 seconds, see Figure 5.1.

Neon Compressor:
For the neon compressors a pill diameter of 13.4 mm and an insulation thickness 2 mm are chosen. These dimensions also add up to 17.4 mm. A heating time of 72 seconds is chosen, this heating time provides a good compromise between the number of compressor cells and the total input power of the system, see Figure 5.3. The compressor system will include 11 compressor cells and requires 184 W input power. Each compressor in this system has a cycle time of 635 seconds.

Hydrogen Compressors:
The compressors in both stages of the hydrogen compressor system have the same dimensions as the neon compressors. Both stages include six compressor cells to operate. The compressors in the low pressure stage of the hydrogen compressor systems will heat for 43 seconds, which corresponds with a cycle time of 459 seconds. The compressors in the high pressure stage of the hydrogen compressor system will heat for 44 seconds, which corresponding with a cycle time of 396 seconds. The total hydrogen stage requires an input power of 185 W.

The total sorption compressor system for the METIS cooler, using sorption compressors with an insulation layer, requires 63 compressor cells and 994 W of input power. An extra margin of 10% on each individual compressor stage increases the number of compressor cells to a total of 70 and the input power to 1093W. The total input power of the compressor system would be 832 W if sorption compressors with a gas-gap heat switch are used, see Table 1.2.

Replacing the gas-gap heat switch in these sorption compressor cells by a layer of insulation will increase the input power of the compressor system for the METIS cooler by 31%. However, this new design will increases the manufacturability and lower the production cost of the compressor cells.

Stage	*Neon*	*Hydrogen - Low*	*Hydrogen - High*	*Helium*
Pill Diameter (mm)	13.4	13.4	13.4	15.0
Insulation Thickness (mm)	2	2	2	1.2
Heating Time (s)	72	43	44	11.8
Cycle Time (s)	635	459	396	112
Number of Cells	11	6	6	40
Input Power (W)	184	85	100	625
Number of Cells (10% margin)	12	7	7	44
Input Power (W) (10% margin)	202	94	110	687

Table 5.1: Optimized compressor cell parameters of the new compressor systems in the METIS cooler.

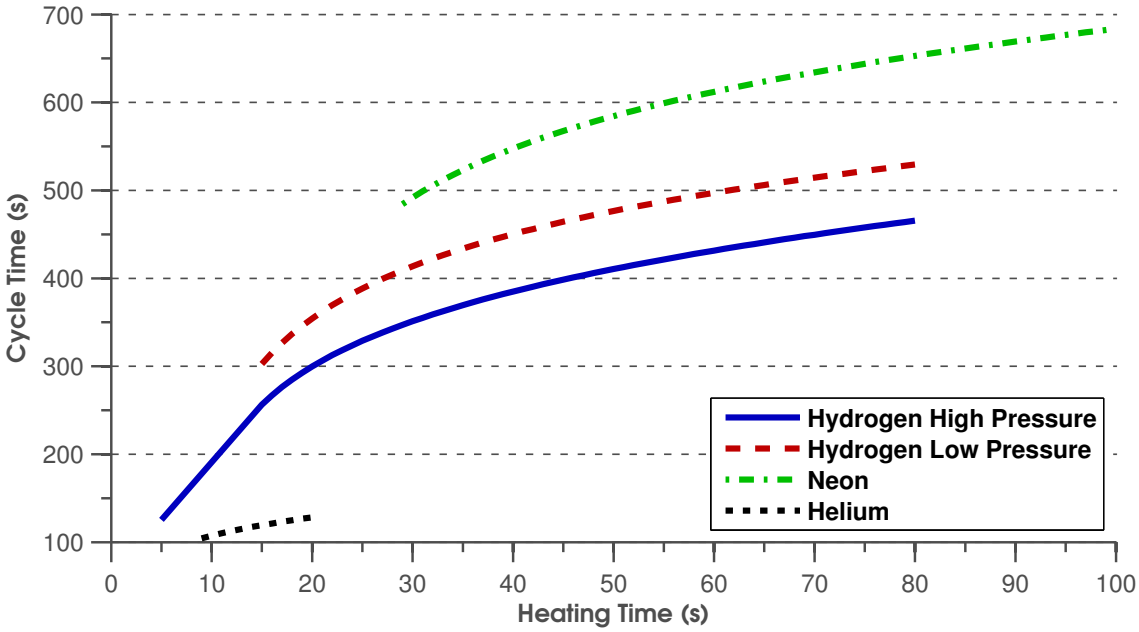

Figure 5.1: Cycle time as a function of the heating time for the different compressors.

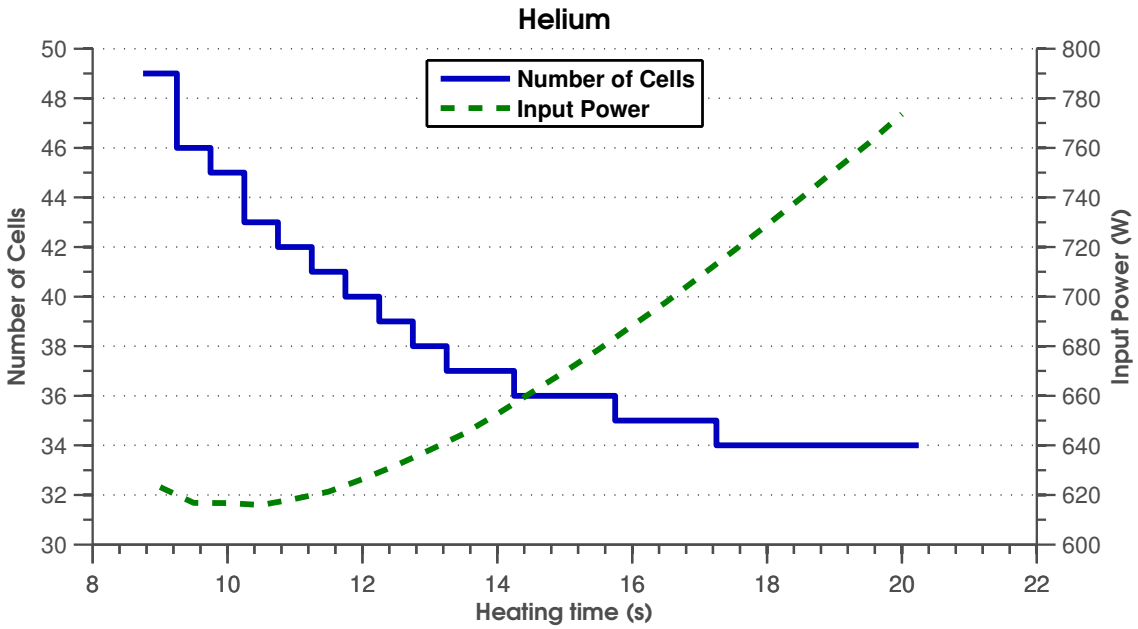

Figure 5.2: The total input power and number of cells for the helium compressor system as a function of the heating time.

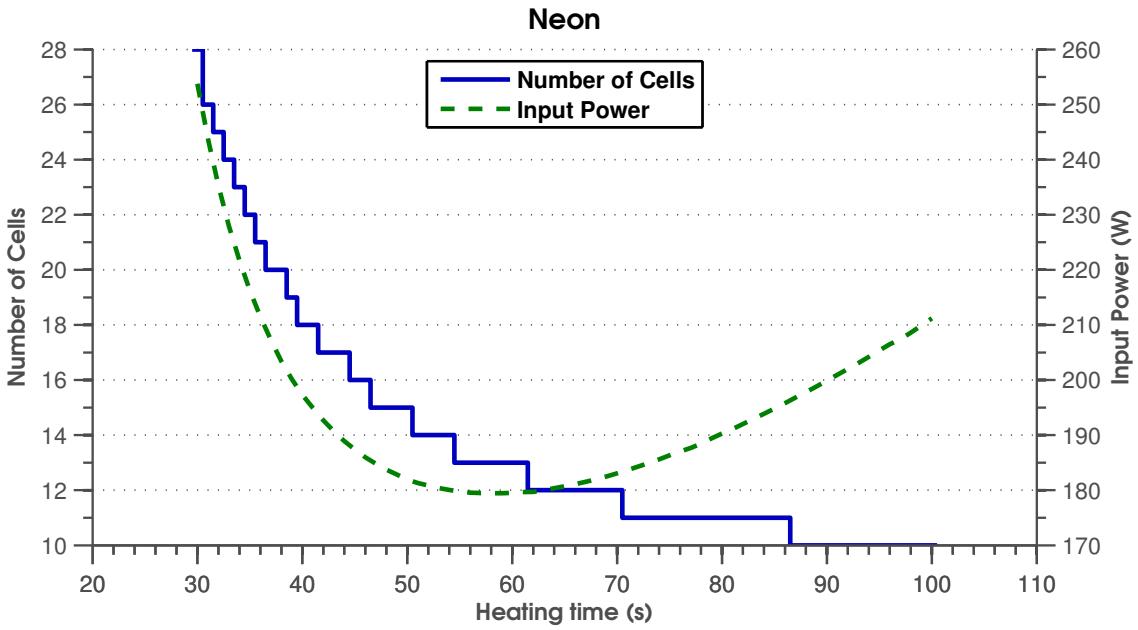

Figure 5.3: The total input power and number of cells for the neon compressor system as a function of the heating time.

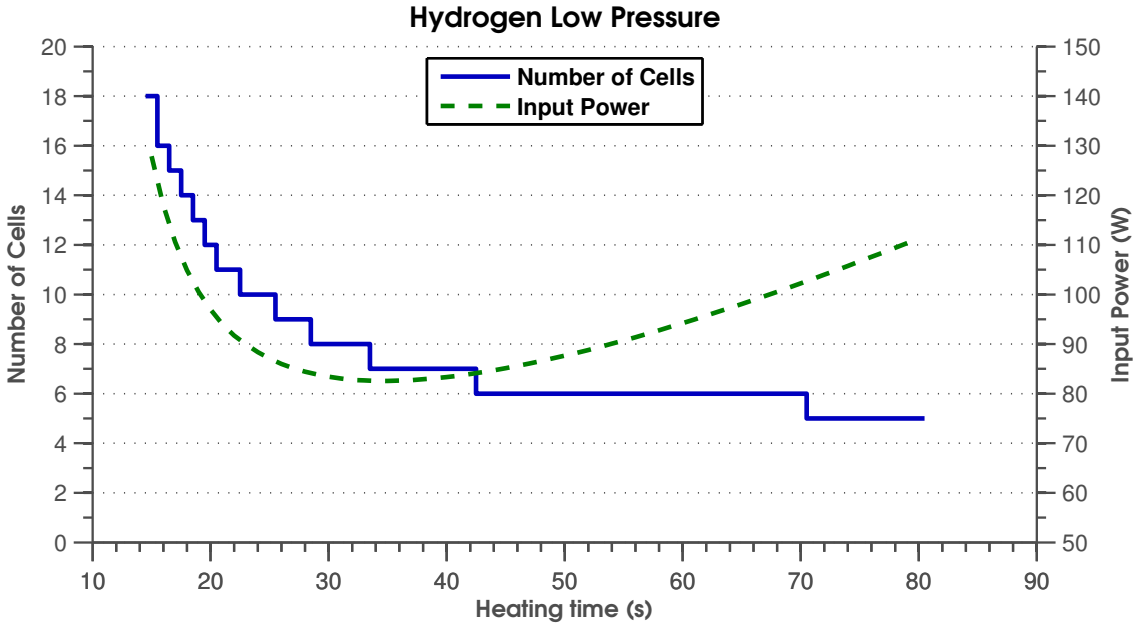

Figure 5.4: The total input power and number of cells for the low pressure hydrogen compressor system as a function of the heating time.

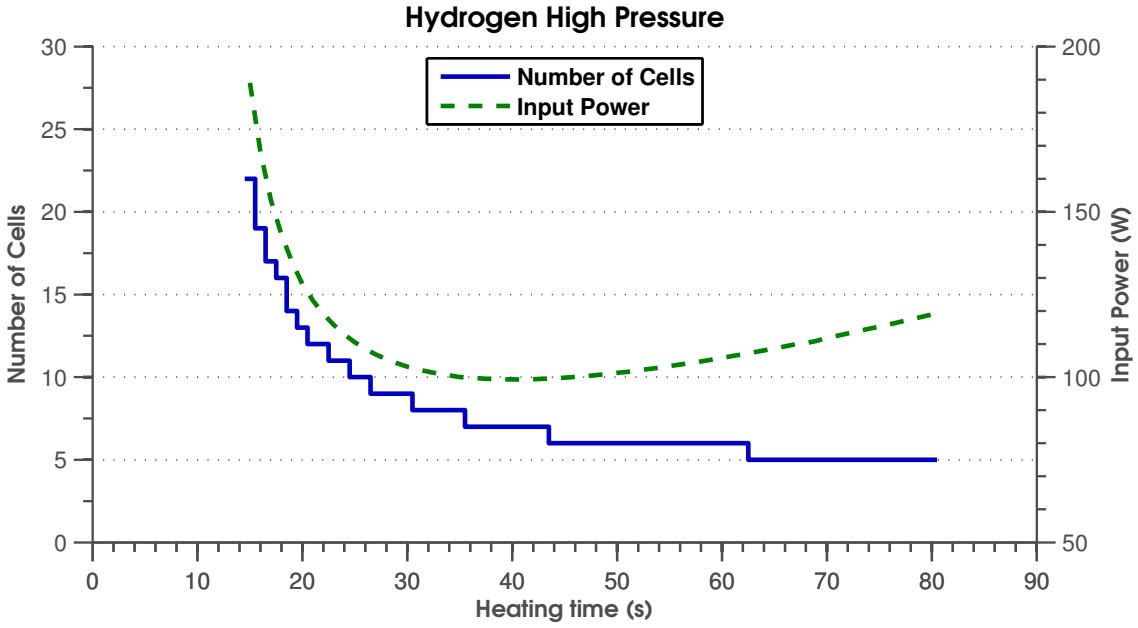

Figure 5.5: The total input power and number of cells for the high pressure hydrogen compressor system as a function of the heating time.

6 Conclusions

A dynamic thermal model is developed to predict the performance of sorption compressors with a layer of insulation and to design four new compressor systems for the METIS cooler. This model has been validated by two different experiments, proving the results of the model are valid to use in the design of actual compressor cells.

Parametric variation has been used to optimize the geometric and operating parameters for the compressor cells in the different compressor systems. The optimization of the compressor system yielded the following systems:
Neon compressor system: 11 compressor cells and 184 W input power.
Two-Stage Hydrogen compressor system: 12 compressor cells and 185 W input power.
Helium compressor system: 40 compressor cells and 625 W input power.

If an extra 10% margin is included in all four stages, the total compressor system for the METIS cooler will consist of 70 compressor cells and that requires a total input power 1093 W. This is a 31% increase in input power compared to a compressor system that uses compressors with a gas-gap heat switch *Thus by replacing the gas-gap heat switch by a layer of insulation reduces the efficiency of the compressor cells, but brings better manufacturability and lower production costs.*

In addition, simulations show that by adding thin sheets of aluminium between the carbon pills the average mass-flow per cell can be increased without increasing the input power of a compressor system. This can lead to 20% less cells per compressor system and thus the production of cheaper compressor systems that take up less space.

The total design of the compressor system still has to be finalized. A choice has to be made between buffers with activated carbon inside or larger buffers without carbon and the corresponding filling pressures have to be calculated. Also a choice has to be made if multiple compressor cells will be grouped; less check valves are needed, but if one compressor malfunctions, the performance whole group decreases. At the moment, the current focus lays on the production of a working helium cold stage and, hopefully, in the near future the first compressor cells with the insulation layer will be build and tested.

Acknowledgements

This project gave me a great insight to the world of sorption compressors, micro-cooling and cryogenics in general. I have learned a lot about the technical aspects of cooler design and thermal modeling. This was the first time I could use finite element modeling and object-orientated modeling combined while having the opportunity to challenge and improve my programming abilities.

In the first place I would like to thank Roger Wu and Marcel ter Brake for their guidance during my time here. I would like to thank Cris Vermeer and Harry Holland for helping me with the experiments and the technical aspects of my work. I also would like to thank Edwin, Haishan, Srini and all of the above for the educational discussions during the cooler meetings. Of course I cannot leave without thanking all other people in the EMS group for all the pleasant conversations during the coffee breaks and drinks.

And finally, I would like to thank my girlfriend for her support and for being on an internship in New Zealand during the last few months of my work, otherwise I could not have finished my thesis in time.

References

[1] Wiegerinck G.F.M. et al., *Thermodynamic optimization of sorption-based Joule-Thomson coolers.*, Cryogenics 47, 143-152, 2007

[2] De Waele A.T.A.M, *Basic Operation of Cryocoolers and Related Thermal Machines*,Review article, J. Low Temp. Physics, Vol.164, pp.179-236, 2011

[3] Maytal B.Z and Pfotenhauer J.M, *Miniature Joule-Thomson Cryocooling, principles and practice*, Google books, web 24 Feb. 2014, http://books.google.com/books?id=XVbLZOF6kqwC

[4] Wade L.A. et al., *Hydrogen Sorption Cryocoolers for the Planck Mission*, Advances in cryogenic engineering, 1999

[5] Burger J.f. et al., *Long-life vibration-free 4.5 Kelvin sorption cooler for space applications*, Rev. Sci. Instrum. 78, 065102, 2007

[6] European Southern Observatory (ESO), Web 20 Dec. 2013, http://www.eso.org/

[7] Ramsay S. et al, *An overview of the E-ELT instrumentation programme*, Proc. of SPIE Vol. 7735 773524, 2010

[8] Kasper M.E. et al., *EPICS, the exoplanet imager for the E-ELT*, Proc. of SPIE Vol. 7015 70151S, 2008

[9] Davies R. et al., *MICADO: the E-ELT Adaptive Optics Imaging Camera*, Proc. of SPIE Vol. 7735 77352A, 2010

[10] Evans C.J. et al., *Science Requirements for EAGLE for the E-ELT*, Proc. of SPIE Vol. 7014 701462, 2008

[11] B. R. Brandl et al., *Instrument Concept and Science Case of the mid-IR E-ELT Imager and Spectrograph METIS*, 2010

[12] Ter Brake H.J.M. et al., *Sorption-based vibration-free cooler for the METIS instrument on E-ELT*, Proc. of SPIE Vol. 8446, 84467O, 2012

[13] Bansal R.C., 2010, *Activated Carbon Adsorption*, Google books. Web 20 Dec. 2013, http://books.google.com/books?id=juWnY_9VkCoC

[14] Wu Y., Technical Notes on the METIS cooler chain, University of Twente

[15] Benford D. et al., *Thermal conductivity of Kapton tape*, Cryogenics, Volume 39, Issue 1, 1999, Pages 93-95

[16] Agrawal V., Web 17 July 2013, http://systemsbiology.us/

[17] Harier E. et al., *Stiff differential equations solved by Radau methods*, Journal of Computational and Applied Mathematics, Volume 111, Issues 1-2, 93-111, 1999

[18] Ekin J., *Experimental Techniques for Low-Temperature Measurements*, Oxford University Press, 2006

[19] NIST Reference Fluid Thermodynamic and Transport Properties Database (REFPROP) 8.0

[20] Nield D. A., 2006, *Convection in Porous Media*, Google books. Web 15 Nov. 2013, http://books.google.com/books?id=tG8sxSHrPEIC

[21] Wiegerinck G.F.M. et al., *Thermodynamic optimization of sorption-based Joule-Thomson coolers*, Cyogenics, Volume 47, Issue 3, 143-152, 2007

[22] Young D. M., *Physical Adsorption of Gases*, Buttersworths, London, 1962

[23] Thermocoax, Web 5 Dec. 2013, http://www.thermocoax.com